Technical report 640/2022/ENG

MONITORING OF THE BRITTLE STRUCTURES ACTIVITY WITHIN THE BUKOV URF AND THE ROŽNÁ MINE – FINAL REPORT AND NUMERICAL MODEL

Authors: Josef Stemberk et al.

Prague, 2022

SÚRAO

This report was prepared in the project financed by SÚRAO. The opinions presented and the conclusions reached are those of the author(s) and do not necessarily represent the views of SÚRAO.

REPORT NAME: Monitoring of the brittle structures' activity in the Bukov URF and the Rožná mine – Final report and numerical model

PROJECT NAME: Monitoring of the brittle structures' activity monitoring in the Bukov URF and the Rožná mine

PROJECT IDENTIFICATION: Final report

CONTRACT NUMBER: SO2018-054

TEAM OF AUTHORS: Stemberk J., Mašín D., Briestenský M., Hartvich F., Fučík Z.

BIBLIOGRAPHICAL REFERENCE: Stemberk J. et al. (2022): Monitoring of the brittle structures' activity in the Bukov URF and the Rožná mine – Final report and numerical model. TZ 640/2022/ENG, SÚRAO, Prague.

Jan Smutek

Project manager (SÚRAO)

Josef Stemberk

Project manager (IRSM CAS)

SÚRAO

Content

Abstract

Final report summarized results of the project „Monitoring of the brittle structures' activity within the Bukov URF and the Rožná Mine", which focused on the monitoring and evaluation of displacements along selected structures during period 2019 – 2022. Ten 3D extensometers TM71 with precision up to 0.001 mm were applied. Displacement data were recorded once per day at 0:00 GMT. Data obtained since the end 2019 till August 2022 indicated trend displacement along some structures with magnitude up to 0.1 mm/y. Compressional regime was identified in May-June 2021, when the relative uplift of the southern blocks was observed. It corresponds to the previous results of fault slip monitoring within the Skalka Gallery about 3 km ESE from the Bukov URF. During 2003 – 2005 several compression periods resulted to the uplift of the southern blocks of about 1 mm (Stemberk et al. 2010). Following analyses of the stress field were performed in "quasi-2D" model, when only the horizontal component of the measured deformations was simulated. Model was constructed as 3D horizontal section around the Bukov URF between levels about -536,5 m and -546.5 m. Software Plaxis 3D VIP was applied for simulation. Using horizontal stress on the individual blocks the back analyses of the measured displacements was performed. The resulting model indicates considerable horizontal stress corresponding to the values determined using different methods in boreholes in the Bukov URF galleries (Souček et al., 2018).

Keywords

Brittle structures, faults, activity, extensometer, micro-displacements, numerical stress model, finite element method, stress, Bukov URF

Abstrakt

Závěrečná zpráva shrnuje výsledky projektu „Monitoring aktivity křehkých struktur PVP Bukov a dolu Rožná", jehož náplní byl monitoring a hodnocení posunů na vybraných strukturách v období 2019–2022. Pro monitoring bylo použito 10 prostorových extenzometrů TM-71 umožňující měřit posun s přesností až 0,001 mm. Měření posunů bylo prováděno s frekvencí jedenkrát za den a to v 0:00 GMT. Data získaná od konce roku 2019 do srpna 2022 naznačují, že na některých strukturách lze identifikovat pohybový trend blížící se hodnotám kolem 0,1 mm/rok. V květnu a červnu 2021 byl identifikován kompresní režim postihující všechny monitorované struktury. Během této komprese byl pozorován relativní zdvih jižně situovaných bloků vůči blokům severním což je v souladu s výsledky měření posunů na strukturách ve štole Skalka cca 3 km VJV od PVP Bukov. V období 2003 – 2005 zde byl identifikován kompresní režim s několika výzdvihy jižně situovaných bloků celkově cca o 1 mm (Stemberk et al., 2010). Pro vyhodnocení monitorovaných posunů byl sestaven „quasi-2D" model PVP Bukov, který byl proveden jako 3D horizontální řez v okolí PVP Bukov v úrovni mezi cca -563.5 m a -546.5 m. Pro simulace byl využit software Plaxis 3D VIP. Aplikací horizontálních tlaků na jednotlivé bloky pak byla snaha o zpětnou analýzu naměřených pohybů. Model ukazuje na výrazné horninové horizontální tlaky jejichž hodnoty odpovídají měření napjatosti různými metodami prezentovanými ve zprávě z geotechnického průzkumu oblasti (Souček et al., 2018).

Klíčová slova

Křehké struktury, zlomy, aktivita, extenzometr, mikroposuny, numerický napjatostní model, metoda konečných prvků, napjatost, PVP Bukov

1 Introduction

This Final Report summarises the results of the project entitled “Monitoring of Activity of Brittle Structures at the Bukov Underground Research Facility and the Rožná Mine”. The objective of the project was to provide monitoring and evaluation of displacements measured from 2019 to 2022 on selected structures identified within the Bukov Underground Research Facility (URF) and their processing using a numeric model to simulate the current state of stress. The interim project results were presented in Technical Reports TZ 526/2020 (Stemberk, Briestenský, Hartvich, Fučík 2020) and TZ 571/2021 (Stemberk, Briestenský, Hartvich, Fučík 2021).

Monitoring was performed with ten TM-71 spatial opto-mechanical extensometers that allow displacement measurement on a discontinuity with an accuracy down to 0.001 mm along each axis. Seven extensometers were installed in the Bukov URF and three in the Rožná mine. After the controlled inundation of lower levels of the Rožná mine started in 2020, these three extensometers were transferred to other identified structures in the Bukov URF. Displacement measurement was made once a day at 00.00 GMT. After instrument reading, the data were transferred by internet to the CAS IRSM for further processing, evaluation and analyses. Regular monitoring was launched in September 2019 and the data presented herein are available up to the end of August 2022.

The final evaluation of displacements monitored during the whole period was performed using the “quasi-2D” model of the Bukov URF, which was made as a 3D horizontal section located in the vicinity of the Bukov URF between approximately -563.5 m and -546.5 m. The back-analysis of the measured displacements was carried out by the application of horizontal pressures on individual blocks. Plaxis 3D VIP software was used for the simulations.

Chapter 2 gives a summary of the methodology for displacement monitoring. Chapter 3 contains descriptions of each monitored structure. The overall results of displacement monitoring along specific structures in the Bukov URF are summarised in Chapter 4. The preparation, description and result of the numeric model are presented in Chapter 5. Chapter 6 summarises the basic evaluation results of monitoring data and numeric modelling. Values of identified displacements on the structures are also subjected to quantitative comparison with foreign as well as domestic sites where long-term fault slip monitoring has been going on. The report concludes with recommendations for the next procedure.

2 Methodology of Active Slip Measurement on Faults

A TM-71 opto-mechanical extensometer (Fig. 1) was used for the monitoring of fault slips and activity of brittle structures in the Bukov URF and the Rožná mine. It is an instrument that measures relative 3D displacement and rotation between two blocks separated by a discontinuity (Fig. 2b; Košťák 1969; Klimeš et al. 2012; Martí et al. 2013). The instrument uses optical interference (Oster and Nishijima 1963) to measure relative displacement. Optical interference (Fig. 2a) appears when two periodical structures, namely spirals, slide over one another, and characteristic interference strips (moiré) occur (Košťák a Popp 1966; Martí et al. 2013). The interference effect can be transformed into a metric system through the number of strips in both fields, i.e., displacement and rotation, and the axis of symmetry (Košťák a Popp 1966). The value of displacement between the centres of glass sheets is determined by the number of interference strips, and the direction of displacement is shown by the main axis of symmetry of the optical effect (Fig. 2d). The application of this effect for the measurement of active tectonic movements was presented, for instance, by Klimeš et al. (2012) and Briestenský et al. (2015, 2018).

The TM-71 extensometer records not only translational displacements between blocks, but also their relative rotation. Its primary advantage is its high accuracy of measurement, reaching down to 0.001 mm. The relative rotation angle is measured with an accuracy of 3.2×10-4 rad (≈0.018°) or better.

The capacities and limits of the extensometer have been tested for a long time at many sites, for instance, in the Czech Republic, Germany, Slovenia, Slovakia, Poland and the Arctic (e.g. Kontny et al. 2005; Gosar et al. 2009; Šebela et al. 2009; Stemberk et al. 2010, 2015). Briestenský et al. (2010) shows that seasonal effects of climatic phenomena can be detected and eliminated from the displacement records. Thermal dilatations and contractions of the TM-71 extensometer are computed and systematically eliminated. Its use for geodynamic monitoring was also tested by comparing the results with those obtained by other monitoring methods, such as horizontal tiltmeters, geodetic surveying, or measurement of underground water level fluctuations (Košťák et al. 2011).

The recorded displacement on a brittle structure can be displayed in the XYZ Cartesian coordinate system or in the SHP system (Košťák, 2006) adopted to the tilt of the measured brittle structure (the s, h, p axis). The computation of displacement and temperature adjustment is described in detail by Košťák (1969). The XYZ Cartesian coordinate system basically displays displacement on the measuring instrument that does not necessarily have to be established perpendicular to the structure or horizontally. In most cases, however, the objective of the installation is to install the measuring instrument perpendicular to the structure or horizontally. With solely vertical structures, both conditions can be maintained. In the Bukov URF, measuring instruments are usually aligned parallel to the gallery, thus the results in the X-axis indicate dilatation of the gallery. Our Final Report includes both raw data in the XYZ system and the adjusted data in the SHP system. In the adapted SHP system, displacements along the h-axis correspond to the horizontal slip and hence represent the strike-slips. The p-axis is perpendicular to the fault plane and the displacement represents the dilatation of the structure. The s-axis is parallel to the fault wall / brittle structure dip direction and represents the subvertical slip (dip slip or reverse slip on the structure). The resulting graphs for each monitoring point contain the values x, y, z (Graph A), rotation along the xy plane and xz plane (Graph B), and the resulting transformation of slips to the plane, i.e., fault dilatation, strike-slip,

and subvertical slip (Graph C). The legends in the diagrams define the direction of movement on the brittle structure.

As data pertaining to air temperature changes in the Bukov URF are available, data on the displacement on brittle structures can be subjected to statistical analysis, and we can look for the relation between displacements and change in air temperature, which also affects the dilatation of the surrounding massif. For a simple analysis, we have used the Pearson correlation coefficient in this Report, which defines the linear correlation between two groups of data. The result can be a positive or negative linear correlation. The closer the value to 1 or -1, the stronger the correlation. According to Evans (1996), the degree of correlation could be very weak (0.00–0.19), weak (0.2–0.39), moderate (0.4–0.59), strong (0.6–0.79) or very strong (0.8–1.00). Air temperature data from the VrK-1 monitoring point (Vylamová et al. 2020) were used for the analysis.

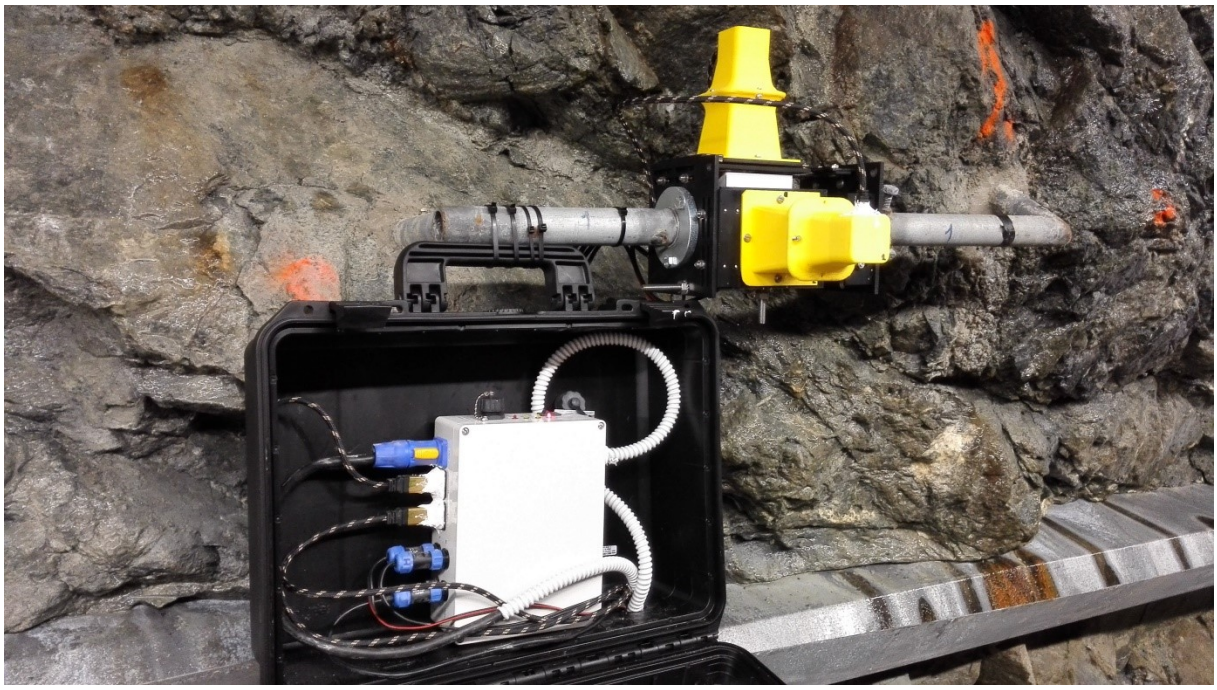

Fig. 1 Extensometer No. 296GWB0001 that is equipped by data-taker.

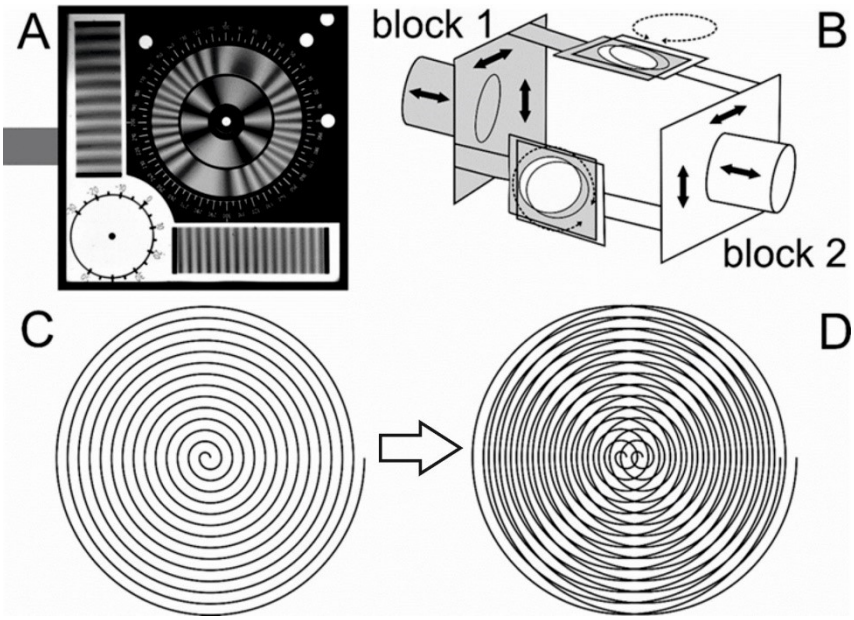

Fig. 2 Opto-mechanical extensometer TM-71 and its basic properties: 3-D movements between two blocks is derived from optical interference, which is registered along three principal axes. A) interference effect arises between two glass sheets obtaining etched spirals; B) schematic sketch of the TM-71 extensometer. Gray parts are connected with block No.1, white parts are fixed in the block No.2. The black arrows display possible displacements; C) etched spiral on the glass sheet; D) two glass sheets overlap generates optical interference.

3 Description of Fault Slip Monitoring Points in the Bukov URF and the Rožná Mine

On the basis of a contract and approval of selected monitoring points, ten points in the Bukov URF and the remaining parts of the Rožná mine were provided with TM-71 extensometers with an automatic logger (Table 1). Two extensometers were installed on the 24th level and one on the 20th level. Seven extensometers were installed in the Bukov URF on selected brittle structures in 2019. No instrument was installed at point no. 3 (296GWB0003) due to ongoing geophysical measurements as part of the "Long-term Monitoring of the Rock Massif in the Bukov URF with Non-destructive Geophysical Methods" project (Bárta et al. 2020) and the possible effects it might have on the measurements in our project, and the point is on hold as one of the potential points for future installation. The instruments from the 20th and 24th levels were removed on 24 June 2020 due to the planned inundation of these levels, and lodged in the overground premises of GEAM Dolní Rožínka. On the basis of an agreement with the Radioactive Waste Repository Authority (SÚRAO), they were subsequently installed on the approved brittle structures in the Bukov URF on 20 January 2021.

Table 1 Overview of the monitored documentary points. Azimuth as well as angle do not match with description of the monitored brittle structures, but they reflect principles of the documentary points tagging in the Bukov URF and other parts of the Rožná mine (it is used for documentary points localisations in the profile of the underground work).

Monitoring point number	**Section of the mine**	**Stationing** (m)	**Azimuth** (°)	**Angle** (°)	**Monitoring period** (from-till)
296GWB0001	BZ_1-XII	70	355	80	9/2019 – 8/2022
296GWB0002	ZK-2	20	90	270	9/2019 – 8/2022
296GWB0004	BZ-XIIJ	220	220	90	9/2019 – 8/2022
296GWB0005	BZ-XIIJ	202	40	280	9/2019 – 8/2022
296GWB0006	BZ-XIIJ	200	40	280	9/2019 – 8/2022
296GWB0007	BZ-XIIJ	170	220	90	9/2019 – 8/2022
296GWB0008	ZK-1	25	355	80	9/2019 – 8/2022
296GWB0009	PŠ1-242	50	223	270	9/2019 – 6/2020
296GWB0010	RV124-83	2	360	270	9/2019 – 6/2020

296GWB0011	Z3-XX	200	170	270	9/2019 – 6/2020
296GWB0012	BZ-XIIJ	269	40	270	1/2021 – 8/2022
296GWB0013	BZ-XIIJ	92,5	40	280	1/2021 – 8/2022
296GWB0014	BZ-XIIJ	22	40	280	1/2021 – 8/2022

296GWB0001

- 12th level, BZ_1-XII laboratory gallery, stationing: 70 m (Fig. 3)
- Monitored brittle structure: 1st order secondary discontinuity, longitudinal, wavy, smooth, closed, filled with tectonic clay, water-bearing, 156/45 (dip direction / dip), striation 064/10 (according to the methodology in Horák 2006)
- The brittle structure character under the requirements as per the contract for work, Annex 3: ii, v, vi, vii (Table 2)
- Northern BZ1-XII gallery wall
- First measurement on 26/09/2019
- Internet data transfer

Table 2 Requirements for monitored brittle structures as per contract SO2018-054.

.i.	Regional fault zone; anticipated site: 12th, 18th or 20th level of the Rožná mine
ii.	Water-bearing fault zone, breadth of up to 3 m, with a continuous water discharge; anticipated site: the Bukov URF
iii.	Fault perpendicular to the identified stress; anticipated site: the Bukov URF, 12th level, or deep levels of the Rožná mine (places with identified orientation of the tensor of stress)
iv.	Fault parallel to the identified stress; anticipated site: the Bukov URF, 12th level, or deep levels of the Rožná mine (places with identified orientation of the tensor of stress)
v.	Fault oblique to the identified stress; anticipated site: the Bukov URF, 12th level, or deep levels of the Rožná mine (places with identified orientation of the tensor of stress)
vi.	Crack zone (smaller-scale brittle structure); anticipated site: the Bukov URF
vii.	Sites 7, 8, 9 and 10 – near the Bukov URF projects (Interaction Experiment, Crack Connectivity) to identify the effects of these experiments on the rock environment.

296GWB0002

- 12th level, ZK-2 gallery, stationing: 20 m (Fig. 3)
- Monitored brittle structure: 1st order secondary discontinuity, longitudinal, wavy, smooth, closed, filled with tectonic clay and breccia, without water-bearing, 100/58 (dip direction / dip), striation 020/5 (according to the methodology in Horák 2006)
- The brittle structure character under the requirements as per the contract for work, Annex 3: i., iv., vii. (Table 2)
- Eastern ZK-2 gallery wall
- First measurement on 11/09/2019
- Internet data transfer

296GWB0004

- 12th level, BZ-XIIJ laboratory gallery, stationing: 220 m (Fig. 3)
- Monitored brittle structure: 1st order secondary discontinuity, longitudinal, wavy, rough, closed, filled with tectonic clay, without water-bearing, 130/60 (dip direction / dip)
- The brittle structure character under the requirements as per the contract for work, Annex 3: v, vi (Table 2)
- Southwestern BZ-XIIJ gallery wall
- First measurement on 24/09/2019
- Internet data transfer

296GWB0005

- 12th level, BZ-XIIJ laboratory gallery, stationing: 202 m (Fig. 3)
- Monitored brittle structure: 1st order secondary discontinuity, longitudinal, wavy, rough, closed, without infill, water-bearing, 350/98 (dip direction / dip), horizontal striations, dextral
- The brittle structure character under the requirements as per the contract for work, Annex 3: ii, iii (Table 2)
- Northeastern BZ-XIIJ gallery wall
- First measurement on 24/09/2019
- Internet data transfer

296GWB0006

- 12th level, BZ-XIIJ laboratory gallery, stationing: 200 m (Fig. 3)
- Monitored brittle structure: 1st order secondary discontinuity, longitudinal, wavy, rough, closed, filled with tectonic breccia, without water-bearing, 140/76 (dip direction / dip)
- The brittle structure character under the requirements as per the contract for work, Annex 3: v, vi (Table 2)
- Northeastern BZ-XIIJ gallery wall
- First measurement on 24/09/2019
- Internet data transfer

296GWB0007

- 12th level, BZ-XIIJ laboratory gallery, stationing: 170 m (Fig. 3)
- Monitored brittle structure: primary discontinuity with secondary activation, 2nd order, longitudinal, wavy, rough, closed, filled with tectonic clay and breccia, without water-bearing, 220/55 (dip direction / dip)
- The brittle structure character under the requirements as per the contract for work, Annex 3: iii (Table 2)
- Southwestern BZ-XIIJ gallery wall
- First measurement on 12/09/2019
- Internet data transfer

296GWB0008

- 12th level, BZ-XIIJ laboratory gallery, ZK-1 Eye, stationing: 25 m (Fig. 3)
- Monitored brittle structure: 2st order primary discontinuity, longitudinal, wavy, rough, closed, filled with tectonic breccia, without water-bearing, 220/68 (dip direction / dip)
- The brittle structure character under the requirements as per the contract for work, Annex 3: v, vi (Table 2)
- Northern ZK-1 gallery wall
- First measurement on 24/09/2019
- Internet data transfer

296GWB0012

- 12th level, BZ-XIIJ laboratory gallery, stationing: 269 m (Fig. 3)
- Monitored brittle structure: 1st order secondary discontinuity, longitudinal, wavy, rough, closed, without infill, without water-bearing, 360/72 (dip direction / dip)
- The brittle structure character under the requirements as per the contract for work, Annex 3: iii (Table 2)
- Northeastern BZ-XIIJ gallery wall
- First measurement on 20/01/2021
- Internet data transfer

296GWB0013

- 12th level, BZ-XIIJ laboratory gallery, stationing: 92,5 m (Fig. 3)
- Monitored brittle structure: 1st order secondary discontinuity, longitudinal, wavy, rough, closed, without infill, without water-bearing, 170/75 (dip direction / dip)
- The brittle structure character under the requirements as per the contract for work, Annex 3: iii (Table 2)
- Northeastern BZ-XIIJ gallery wall
- First measurement on 20/01/2021
- Internet data transfer

296GWB0014

- 12th level, BZ-XIIJ laboratory gallery, stationing: 22 m (Fig. 3)
- Monitored brittle structure: 1st order secondary discontinuity, longitudinal, wavy, rough, closed, filled by tectonic breccia, without water-bearing, 115/60 (dip direction / dip)
- The brittle structure character under the requirements as per the contract for work, Annex 3: iv., vi. (Table 2)
- Northeastern BZ-XIIJ gallery wall
- First measurement on 20/01/2021
- Internet data transfer

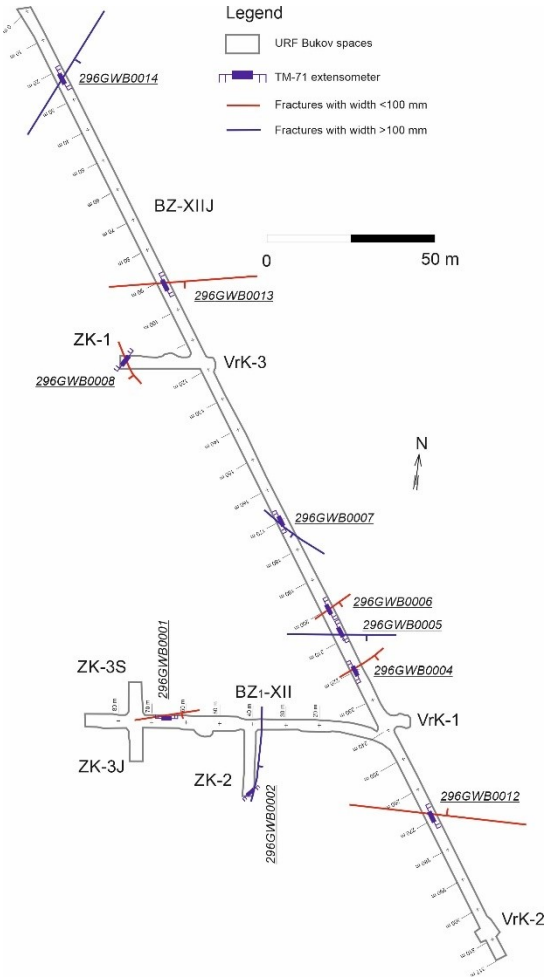

Fig. 3 Monitored sites with TM-71 extensometers and selected brittle structures in the Bukov URF.

296GWB0009

- R1 (previous marking of the monitoring site that was installed in 2012)
- 24th level, PŠ1-242 gallery, stationing: 50 m (Fig. 4)
- Monitored brittle structure: 1st order secondary discontinuity, longitudinal, wavy, rough, closed, filled by tectonic breccia, without water-bearing, 330/85 (dip direction / dip)

- The brittle structure character under the requirements as per the contract for work, Annex 3: v., vi. (Table 2)
- Southwestern PŠ1-242 gallery wall
- First measurement on 11/09/2019
- Monitoring stopped on the 24/06/2020 due to planned inundation of the lower situated levels
- Without Internet data transfer

296GWB0010

- R2 (previous marking of the monitoring site that was installed in 2012)
- 24th level, RV1 24-83 gallery, stationing: 2 m (Fig. 4)
- Monitored brittle structure: 1st order secondary discontinuity, longitudinal, wavy, rough, closed, filled by tectonic breccia, without water-bearing, 090/75 (dip direction / dip)
- The brittle structure character under the requirements as per the contract for work, Annex 3: iv., vi. (Table 2)
- Northern RV1 24-83 gallery wall
- First measurement on 11/09/2019
- Monitoring stopped on the 24/06/2020 due to planned inundation of the lower situated levels
- Without Internet data transfer

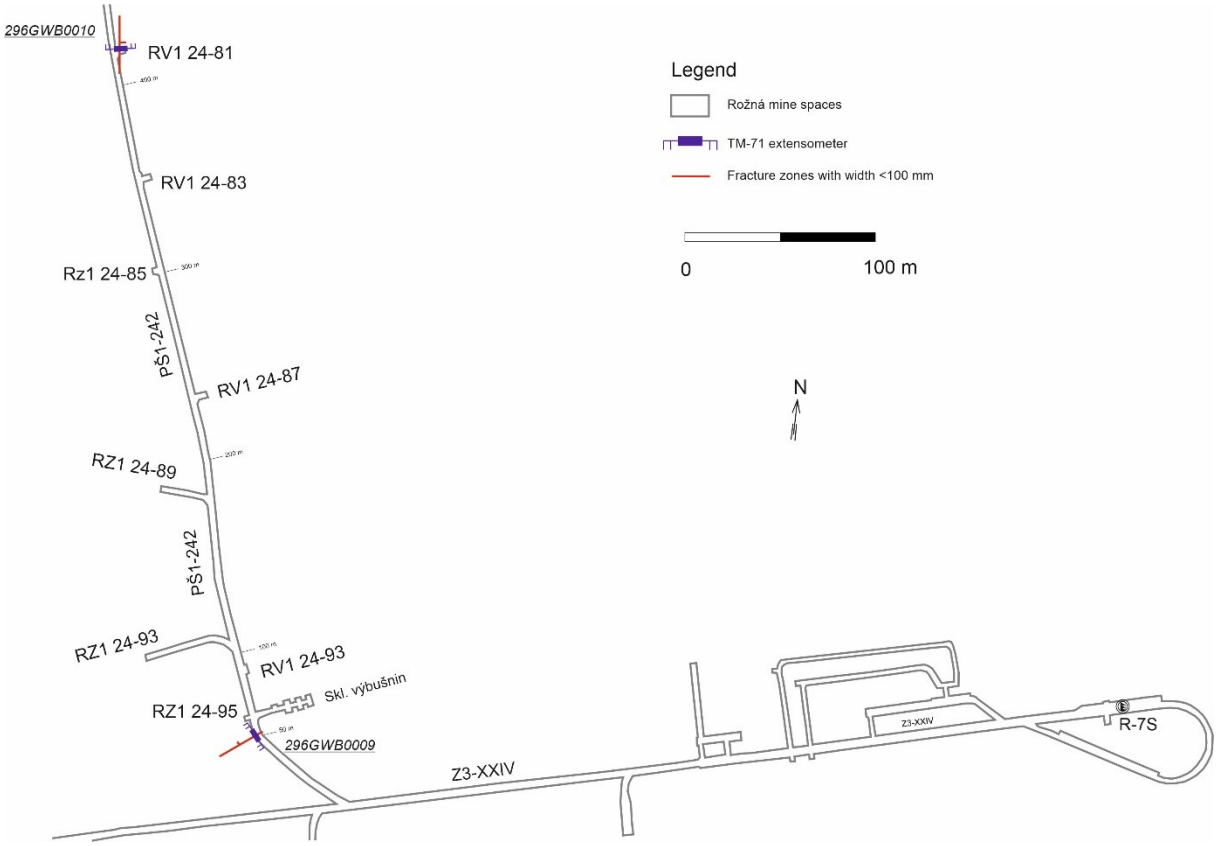

Fig. 4 Monitored sites with TM-71 extensometers and selected brittle structures on the 24th level in the Rožná mine.

296GWB0011

- 20th level, Z3-XX gallery, stationing: 200 m (Fig. 5)
- Monitored brittle structure: 1st order secondary discontinuity, longitudinal, wavy, rough, closed, filled by tectonic breccia, without water-bearing, 180/80 (dip direction / dip)
- The brittle structure character under the requirements as per the contract for work, Annex 3: i., iv. (Table 2)
- First measurement on 12/09/2019
- Monitoring stopped on the 24/06/2020 due to planned inundation of the lower situated levels
- Without Internet data transfer

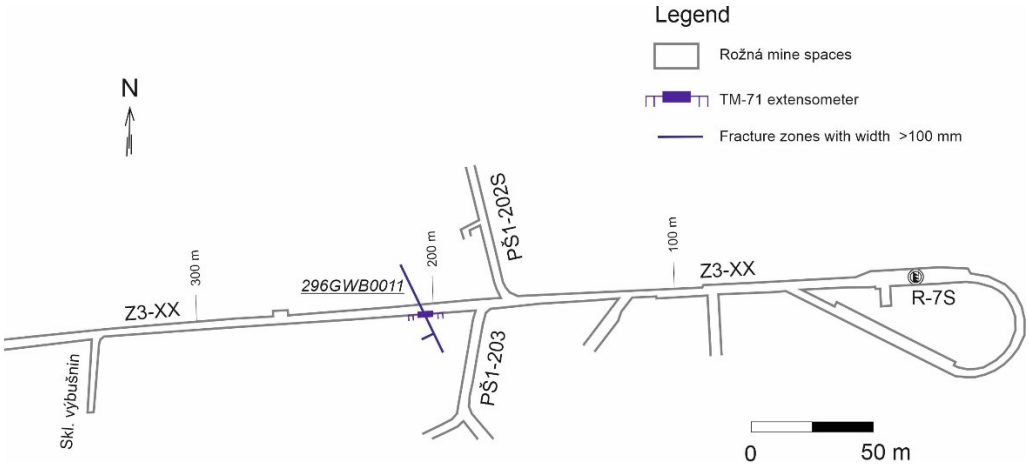

Fig. 5 Monitored site with TM-71 extensometer and selected brittle structure on the 20th level in the Rožná mine.

4 Current Results of Activity of the Brittle Structures

4.1 The 296GWB0001 Monitoring Point

The current results have indicated a significant trend in the subvertical slip of SSE blocks down on the brittle structure. As already presented in the TZ562/2020 report (Stemberk et al. 2020), this trend isn't fluent but consists of short-term pulses/accelerated slips which, according to the latest results, range around hundredths of a mm. This was, for instance, the case with an accelerated slip recorded on 4 September 2020, having the value of 0.034 mm (Fig. 6, Graph C). The subvertical trend according to the current results is 0.1026 mm/yr, approximately one-tenth of a millimetre per year. There is also an apparent low trend in the right-lateral slip here which, during the three years of monitoring, reached 0.026 mm. Concerning the dependence between slips and air temperature at the point VrK-1 (Vylamová et al. 2020), there is no apparent relationship (Fig. 7). With the application of the Pearson correlation coefficient, the correlation for the subvertical slip is moderate (r = 0.50), for the strike-slip it is weak (r = 0.35), and for the brittle structure dilatation it is moderate (r = -0.53). We therefore consider the relation between slips and change in air temperature as lacking evidence.

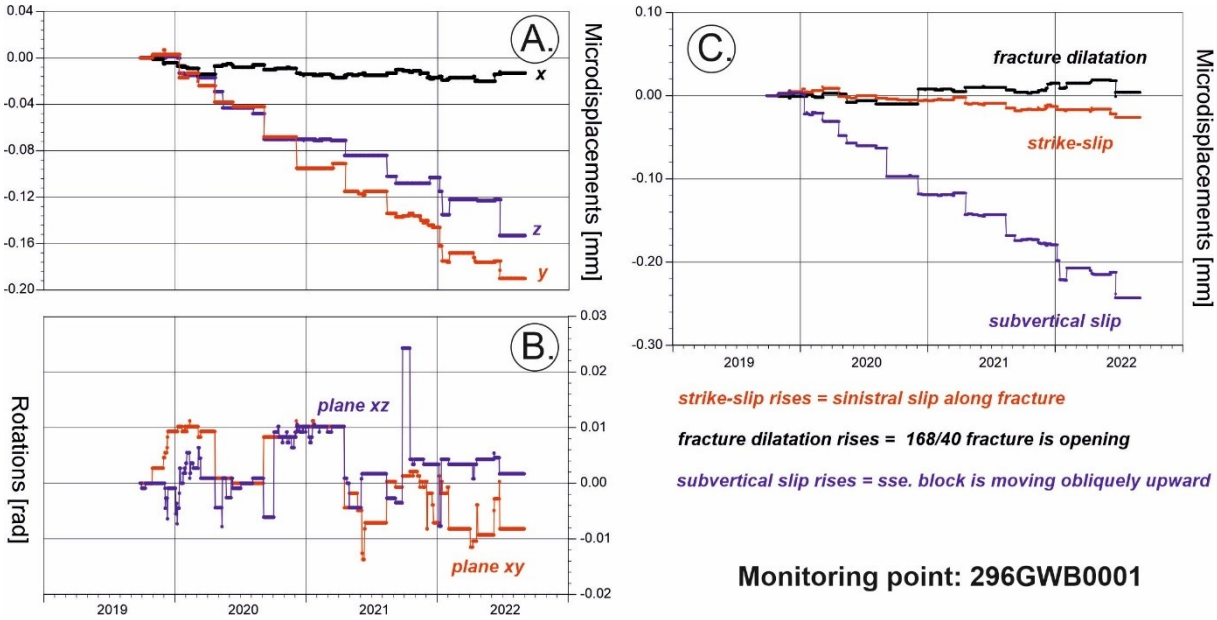

Fig. 6 Extensometric monitoring results at 296GWB0001 site.

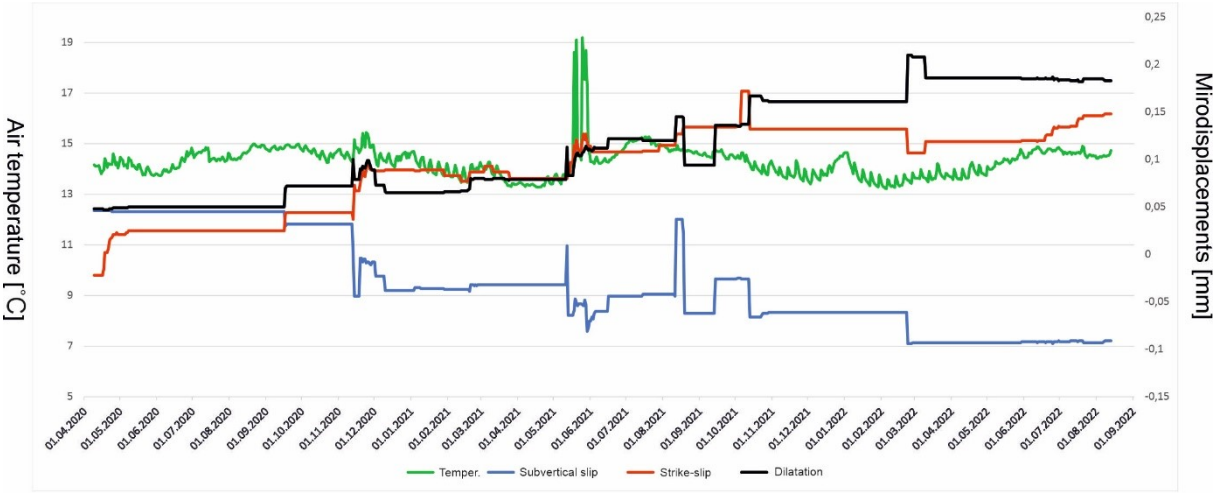

Fig. 7 Air temperature (Vylamová et al. 2020) versus displacements at 296GWB0001 site.

4.2 The 296GWB0002 Monitoring Point

The subvertical slips measured at this point are affected by pulse movements (Fig. 8, Graph C) which are also of reverse character; for instance, the pulse recorded from 10 to 19 August 2021. The strike-slip component already begins to have a right-lateral trend, namely 0.091 mm/yr. Also, the closing of the brittle structure shows a low trend at 0.06 mm/yr which, however, is affected not only by accelerated slips but also the reverse character of the pulses, such as the aforementioned pulse of 10 to 19 August 2021 or that of 22 February – 10 March 2022. Concerning the dependence between slips and air temperature (Vylamová et al. 2020), no apparent relation can be identified here. With the application of the Pearson correlation coefficient, the correlation for the subvertical slip is very weak (r = 0.16), for the strike-slip it is very weak (r = 0.05), and for the fault dilatation it is very weak (r = -0.12). The graph in Fig. 9, however, shows an apparent relation between movements and elevated temperature in the ZK-2 gallery, which relates to the ongoing work on the “Crack Connectivity” project (hydraulic tests; Zuna et al. 2021). After a check of the journal of the Crack Connectivity project, slips which appeared in November 2020 correspond to the drilling in the S-31 borehole. Another prominent movement occurred in May 2021, which also corresponds to the activity in the gallery and increased air temperature (Fig. 9). The aforementioned pulse on 10–19 August 2021, however, does not correspond to elevated temperature or records in the journal. Similarly, the movement occurring on 22 February 2022 was not initiated that way.

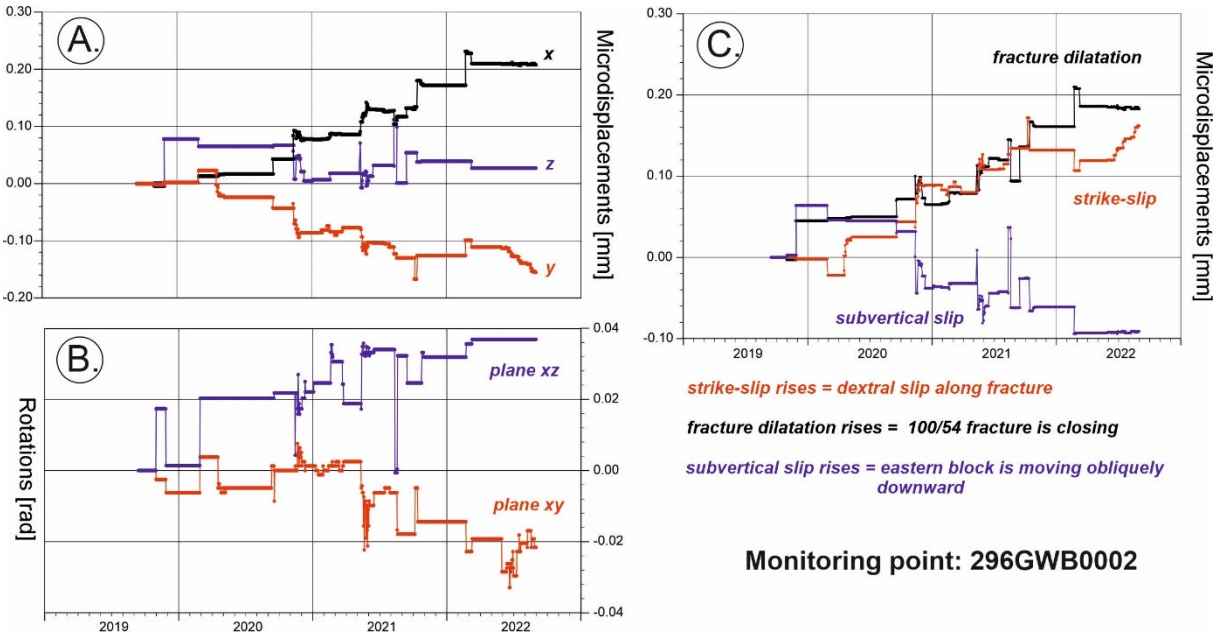

Fig. 8 Extensometric monitoring results at 296GWB0002 site.

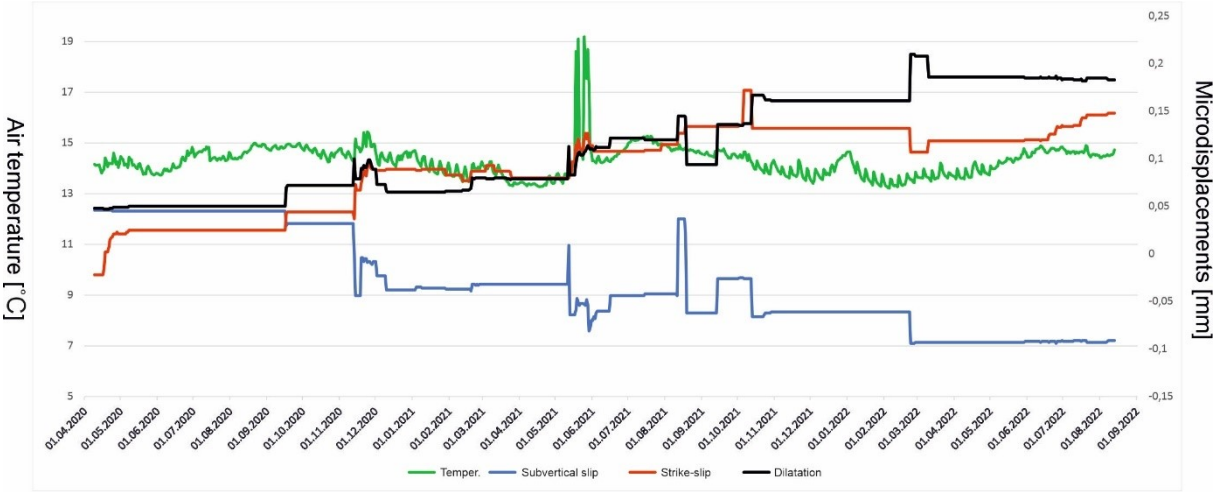

Fig. 9 Air temperature (Vylamová et al. 2020) versus displacements at 296GWB0002 site.

4.3 The 296GWB0004 Monitoring Point

The available results show an apparent trend to a left-lateral strike-slip along the brittle structure here, which can be accelerated for a short period of time, as occurred for instance on 6 November 2019 (see Technical Report TZ 526/2020). So far, the strike-slip trend has been 0.112 mm/yr (Fig. 10). No trends in dilatation of the brittle structure or in subvertical slip are apparent. Both components, however, are affected by a seasonal component resulting probably from the thermal dilatation of the massif, with an amplitude of up to 0.04 mm. This is also documented in Fig. 11, where the monitored X-axis (parallel to the gallery direction) copies the average air temperature obtained at the point VrK-1 (Vylamová et al. 2020). The Pearson correlation coefficient r = 0.86 indicates a very strong correlation.

There was a prominent period of inactivity from 26 June to 7 September 2021. The same period was also observed at other locations within the Bukov URF. Here this period was identified both in dip slips as well as strike-slips along the brittle structure.

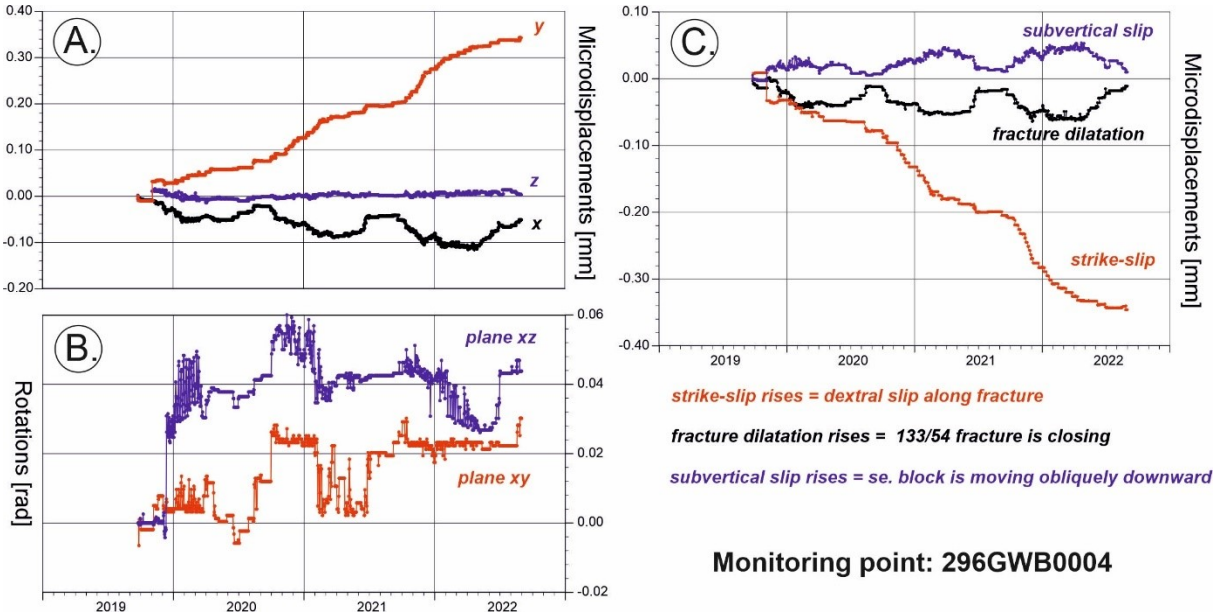

Fig. 10 Extensometric monitoring results at 296GWB0004 site.

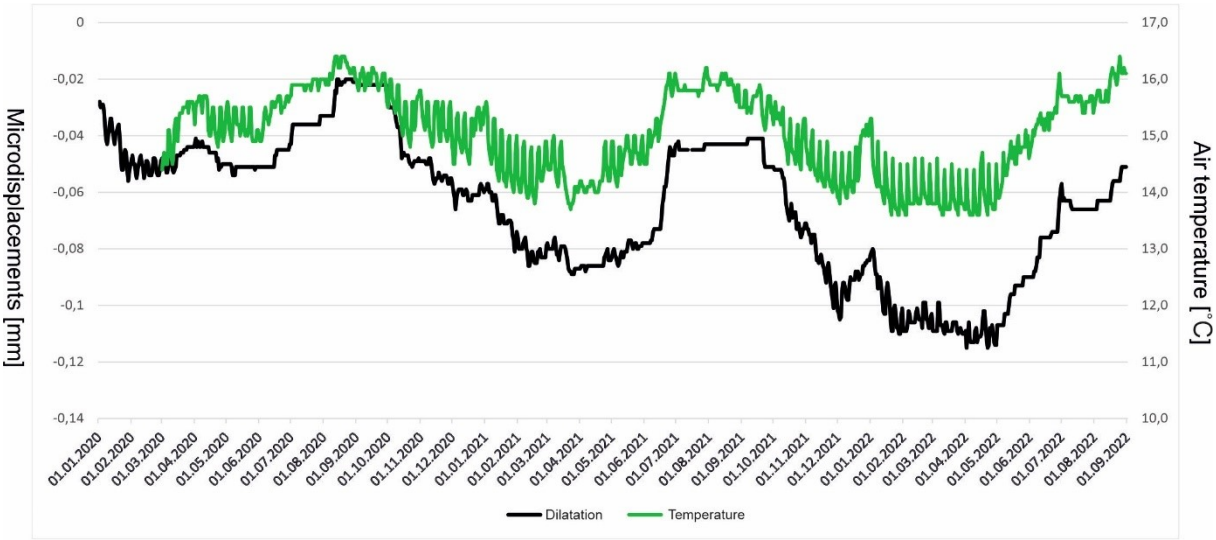

Fig. 11 Air temperature (Vylamová et al. 2020) versus displacements at 296GWB0004 site.

4.4 The 296GWB0005 Monitoring Point

The results obtained so far indicate, as was already presented in the TZ 526/2020 Report (Stemberk et al. 2020), a significant component of fault dilatation. In general terms this is a trend to opening of the brittle structure at 0.017 mm/yr (Fig. 12); this trend is also affected by the seasonal component with an amplitude of approx. 0.03 mm which is probably due to thermal dilatation of the massif. This dependency is documented in Fig. 13, where the

monitored X-axis (parallel to the gallery direction) copies the average air temperature obtained at the point VrK-1 (Vylamová et al. 2020). The Pearson correlation coefficient r = 0.81 indicates a very strong correlation. The data show a sudden reverse slip of the SSE block with a value of 0.022 mm on 18 June 2021, accompanied by right-lateral strike-slip along the brittle structure (Fig. 12, Graph C). The preceding period, however, indicated an opposite trend, i.e., general downslip of the SSE block. We must, however, point out the scale of movements which are in the hundredths of a mm at this point. From 22 June 2021 to 11 October 2021 no movement was recorded (see also the results from the 296GWB0004 point). In 2022 a similar period was observed from 22 January to 13 May. These two periods were followed by a right-lateral strike-slip and also dip slip on the brittle structure.

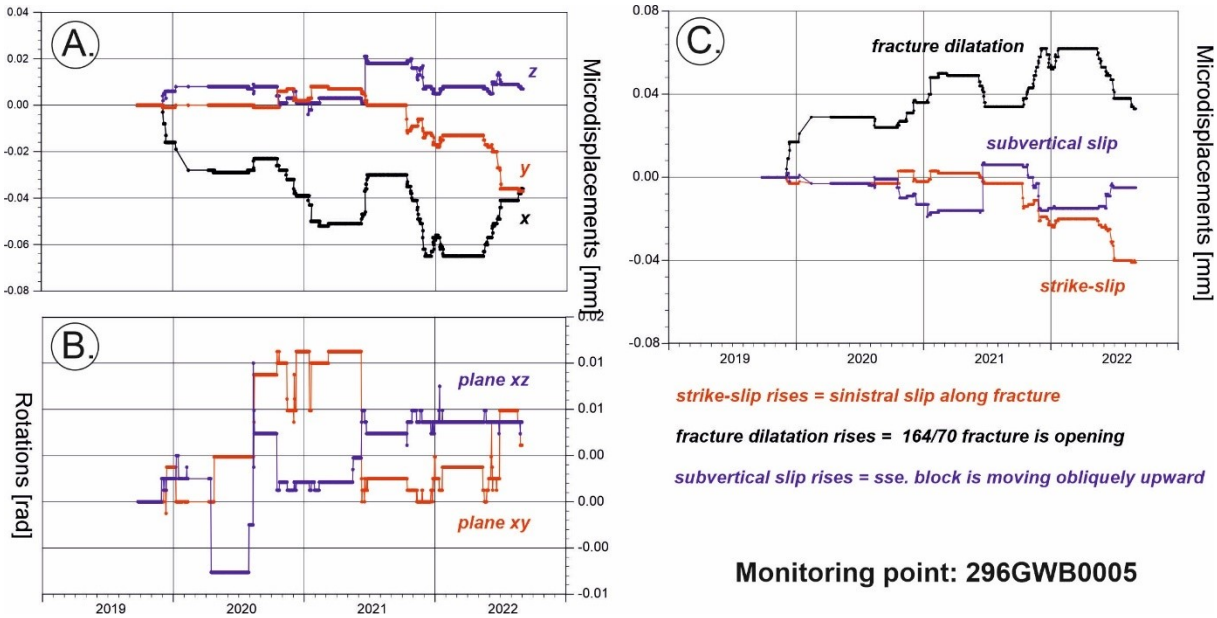

Fig. 12 Extensometric monitoring results at 296GWB0005 site.

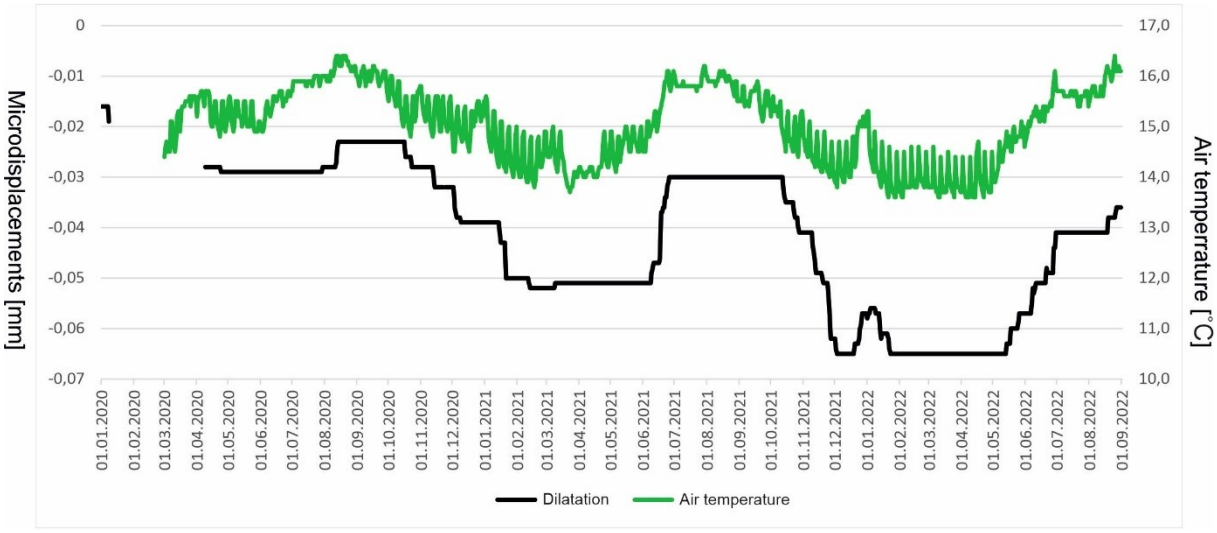

Fig. 13 Air temperature (Vylamová et al. 2020) versus displacements at 296GWB0005 site.

4.5 The 296GWB0006 Monitoring Point

The 296GWB0006 point (Fig. 14, Graph C) indicates trends both in right-lateral strike-slips on the brittle structure and in the closing of the brittle structure. These two components are also affected by the seasonal thermal dilatation with an amplitude of 0.01 mm for the opening of the fault and 0.018 for the strike-slip. The fault closing trend is 0.04 mm/yr, and 0.03 mm/yr for the strike-slip along the brittle structure. However, if we look at the X component (Fig. 14, Graph A), which is parallel to the BZ-XIIJ gallery, the seasonal amplitude of the horizontal dilatation parallel to the gallery is 0.04 mm. The Pearson correlation coefficient r = 0.84 indicates a very strong correlation between the X component and the air temperature at the point VrK-1 (Vylamová et al. 2020). From time to time, movements can also be accelerated, for instance, on 18 April 2020, when a dip slip occurred (the Z component, Fig. 14, Graph A) with a value of 0.038 mm.

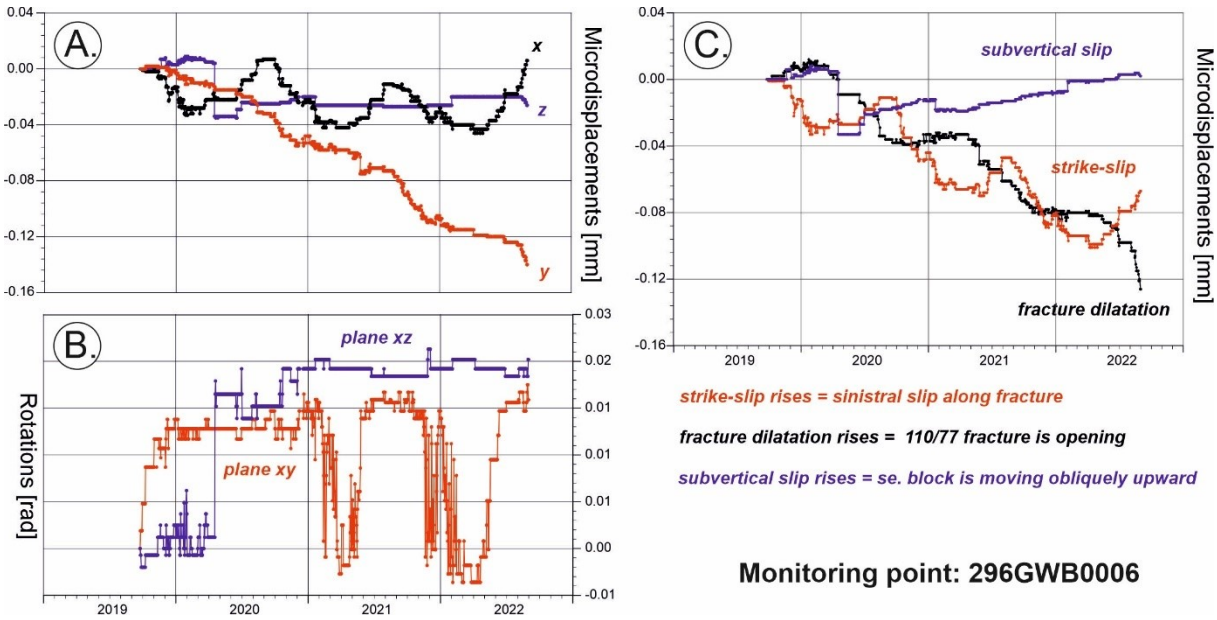

Fig. 14 Extensometric monitoring results at 296GWB0006 site.

4.6 The 296GWB0007 Monitoring Point

Movements at the 296GWB0007 monitoring point follow the trends of the subvertical component and the component of brittle structure dilatation (Fig. 15, Graph C). The subvertical slip trend is 0.09 mm/yr. As already stated in the TZ 526/2020 Report, it is interrupted by significant accelerations or reverse slip, as can be seen, for instance, from May 2021 to the beginning of July 2021. The value of subvertical slip in that period reached 0.095 mm. The trend in brittle structure dilatation is 0.07 mm/yr and can also be influenced by short-term events during which the dilatation movement is reversed against the long-term trends. Such an event occurred in June 2021, when the subvertical slips were also reversed at this point. During that period, reverse slip of the southern block occurred with closing of the fault. So far, the maximum or minimum value in the seasonal amplitude of brittle structure dilatation appears

to be a significant triggering factor for vertical / subvertical accelerations or reversals. This relation is apparent in 2020, 2021 and 2022. Dilatation parallel to the gallery direction (the X component) is influenced by the seasonal component, which is probably due to the thermal dilatation of the massif. This is documented in Fig. 16, where the monitored X-axis (parallel to the gallery direction) copies the average air temperature obtained at the point VrK-1 (Vylamová et al. 2020).The Pearson correlation coefficient r = 0.81 indicates a very strong correlation. The seasonal dilatation amplitude is up to 0.05 mm/yr.

There is also a very prominent period of inactivity from 26 June to 7 September 2021, see above.

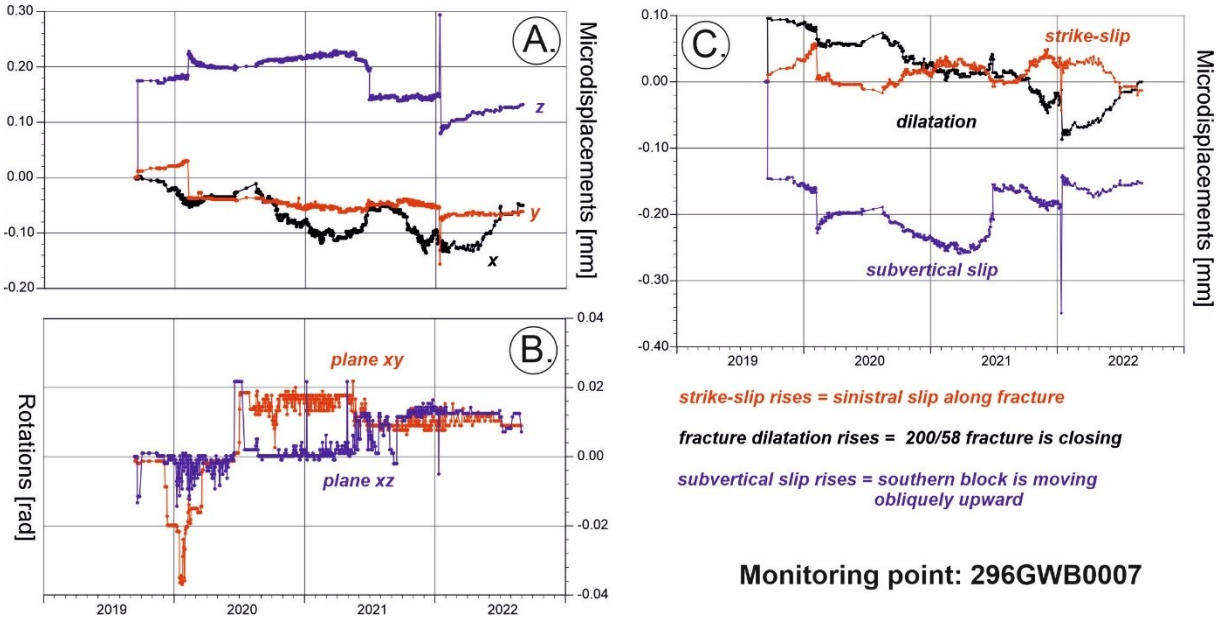

Fig. 15 Extensometric monitoring results at 296GWB0007 site.

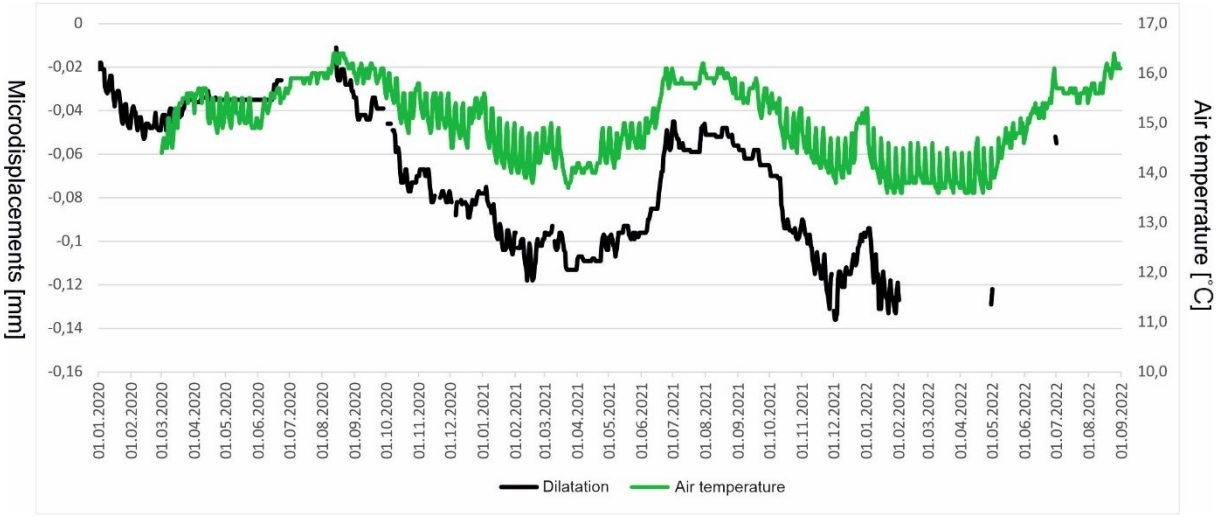

Fig. 16 Air temperature (Vylamová et al. 2020) versus displacements at 296GWB0007 site.

4.7 The 296GWB0008 Monitoring Point

The present results confirmed the sensitivity of the brittle structure, especially to pulse movements (Fig. 17). The latest pulse (on 24 June 2021) was right-lateral slip (0.036 mm) and closing of the structure (0.006 mm). A period of inactivity followed the event here, just like at the aforementioned sites. The pressure period at the end of June 2021 with the subsequent period of inactivity is therefore common for almost the entire Bukov URF. Compared to the results from other locations, no movements bound to the thermal dilatation of the massif are apparent here, and the movements range from hundredths of a mm to thousandths of a mm. Given the size of the movements, this point can be considered stable, and the movements insignificant.

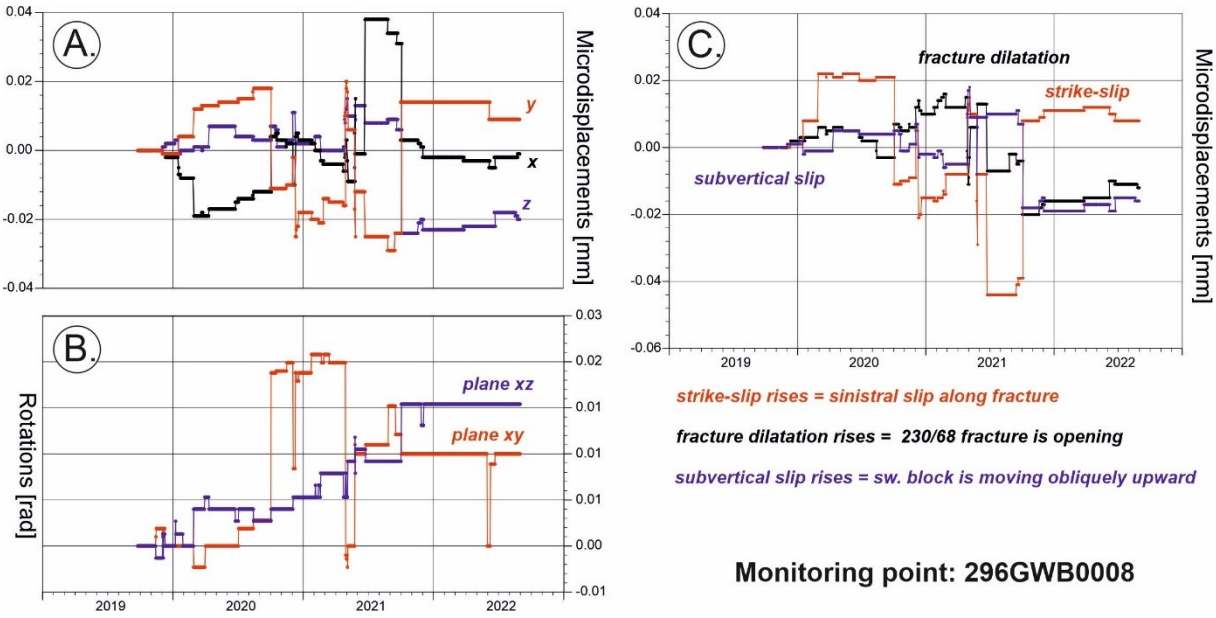

Fig. 17 Extensometric monitoring results at 296GWB0008 site.

4.8 The 296GWB0009 Monitoring Point

In the period from 30 November 2019 to approximately 16 February 2020, the brittle structure was opening at 0.038 mm, with a left-lateral slip of 0.025 mm. After this period, the north-eastern block dip-slipped by 0.065 mm on 20 February 2020. The greatest slip on the brittle structure was therefore this dip slip of the superposed block (Fig. 18, Graph C). This period was followed by a reverse slip of the NW block, or the dip slip of the SE block. At the same time the strike-slip changed from left-lateral to right-lateral and the structure began to close. The subvertical movement was trending until the end of monitoring, as the NW block showed oblique thrust. On 24 June 2020 the instrument was removed due to the decision to inundate the lower levels.

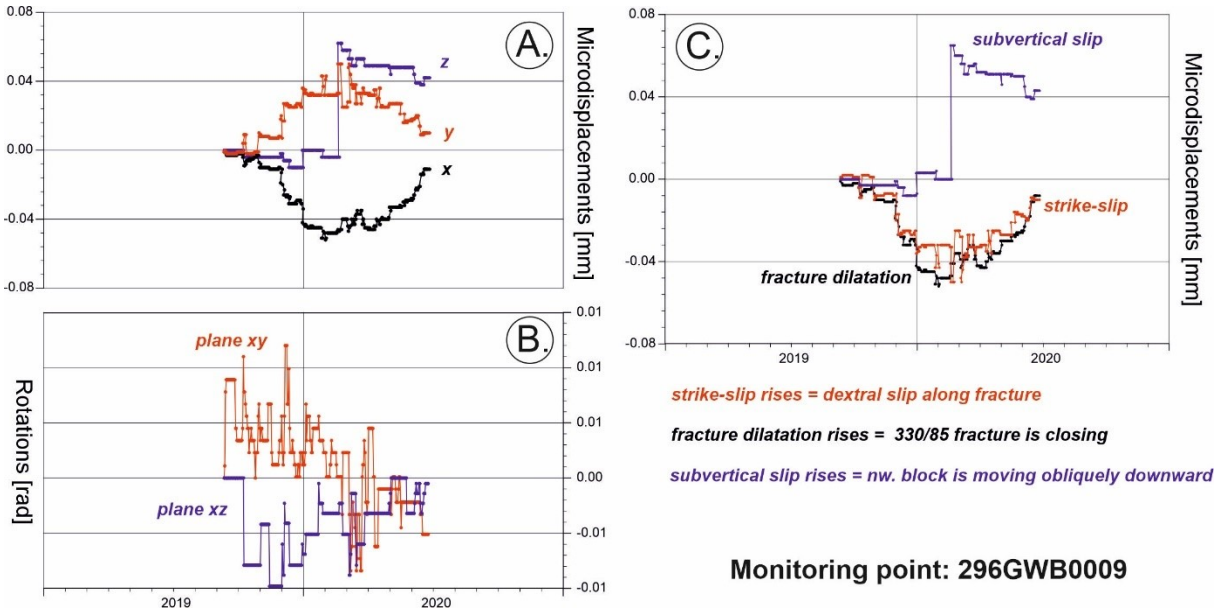

Fig. 18 Extensometric monitoring results at 296GWB0009 site.

4.9 The 296GWB0010 Monitoring Point

From the beginning of the monitoring, the point showed trend slips in all axes. Until 23 January 2020 the E block dip-slipped by 0.013 mm, with a left-lateral slip of 0.016 mm and opening of the structure of 0.036 mm (Fig. 19, Graph C). Opening up was therefore the greatest slip. After this, however, there followed a period with a reverse movement, when the brittle structure was closing, accompanied by a right-lateral slip and a slight reverse slip of the E block. This period continued after an interruption with a short pulse (on 22–27 March 2020) with reverse slips as in the first defined period. Impaired reading of the interference images in the rotations made it impossible for us to evaluate the rotational components of the block movements. This was due to delayed thermal dilatation of the instrument after the installation. The planned rectification of glass sheets to improve the reading of rotations, scheduled for February/March, was cancelled due to the closure of the mine as a quarantine measure. The next scheduled date was already meaningless as the date of the removal of the instrument (24 June 2020) was approaching after a decision to inundate the lower mine levels.

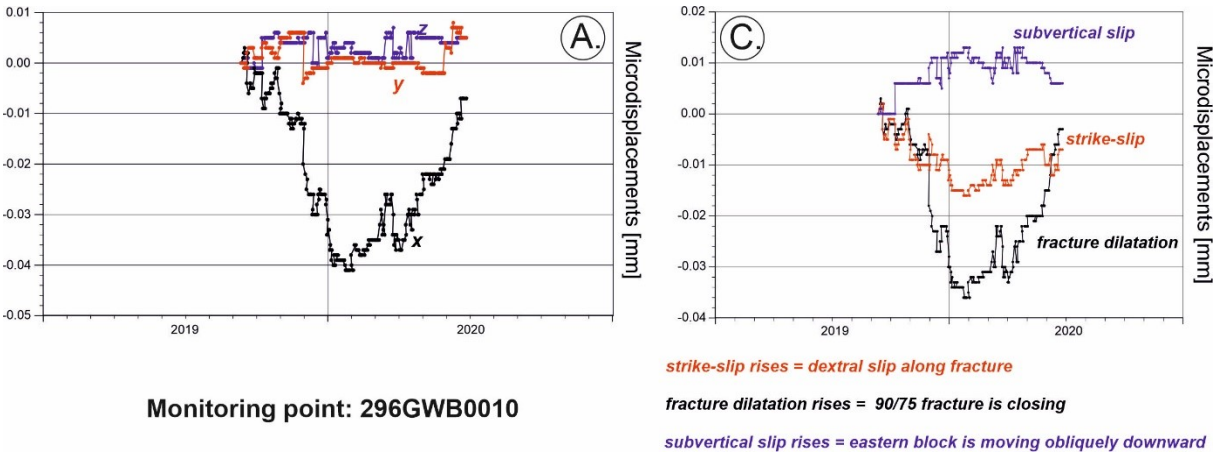

Fig. 19 Extensometric monitoring results at 296GWB0010 site.

4.10 The 296GWB0011 Monitoring Point

A significant movement identified on the monitored brittle structure was a strike-slip and dilatation (Fig. 20, Graph C). From the beginning of the monitoring, there was a left-lateral slip that reached 0.207 mm as of 28 January 2020, and the opening up of the brittle structure reached 0.223 mm. After 30 January we observed a reversal of both the strike-slip (which turned to right-lateral) and the dilatation of the brittle structure (which turned to closing), both of which continued until the end of the monitoring. The strike-slip reached 0.215 mm from 30 January 2020 to 24 June 2020. There was also a short-term significant dip slip of the SW block of 0.066 mm on 25–27 February 2020. This dip slip was followed by a reverse movement, i.e., thrust of the SE block (or dip slip of the opposite NE block) of 0.052 mm from 5 to 8 March 2020. On 24 June 2020 the instrument was removed due to the decision to inundate the lower levels.

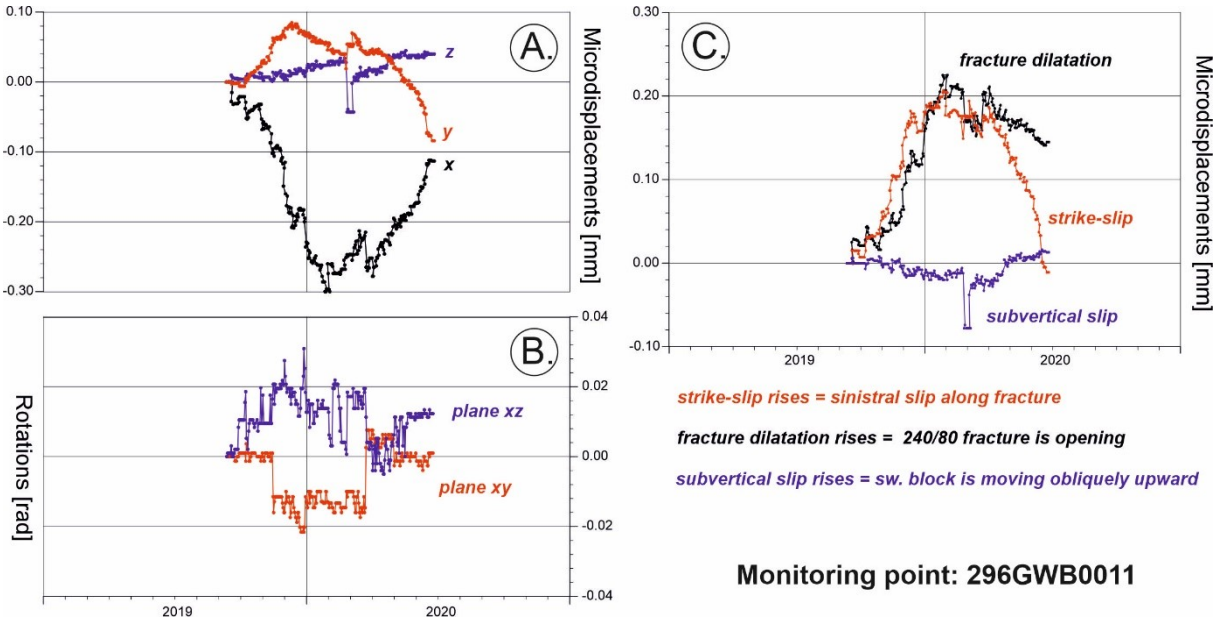

Fig. 20 Extensometric monitoring results at 296GWB0011 site.

4.11 The 296GWB0012 Monitoring Point

With respect to the short monitoring period at this point, the long-term trends on this brittle structure cannot be defined as yet (Fig. 21, Graph C). The results gained so far, however, show an indication of the trends for the dilatation of the brittle structure and strike-slip. Dilatation accelerated on 12 May 2021 by 0.033 mm. After this event, movement in all components ceased. In 2022, a significant right-lateral slip occurred in combination with a dip slip of the N block. This event occurred on 28 June 2022. The strike-slip was 0.049 mm and the subvertical slip was 0.048 mm.

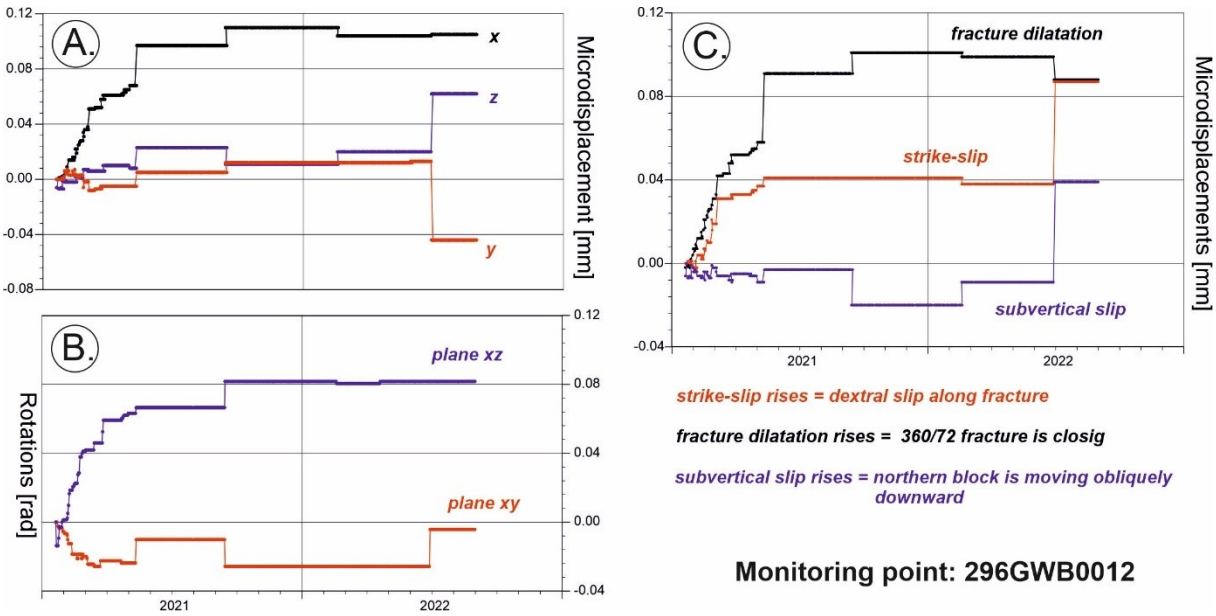

Fig. 21 Extensometric monitoring results at 296GWB0012 site.

4.12 The 296GWB0013 Monitoring Point

All movement components on this brittle structure show a trend that can be accelerated or temporarily attenuated (Fig. 22, Graph C). An acceleration can be seen, for instance, after the beginning of the measurement at the subvertical component and also the strike-slip component. The right-lateral strike-slip had a trend of 0.067 mm/yr in 2021, but accelerated on 22–30 June 2021 by 0.029 mm. After this event, the movements halted. Following that, the trend slightly reversed to left-lateral while the strike-slip ceased in 2022. Further acceleration of movements in all components occurred on 15 August 2022, and the right-lateral slip along the brittle structure became a significant movement. This movement has continued to the present.

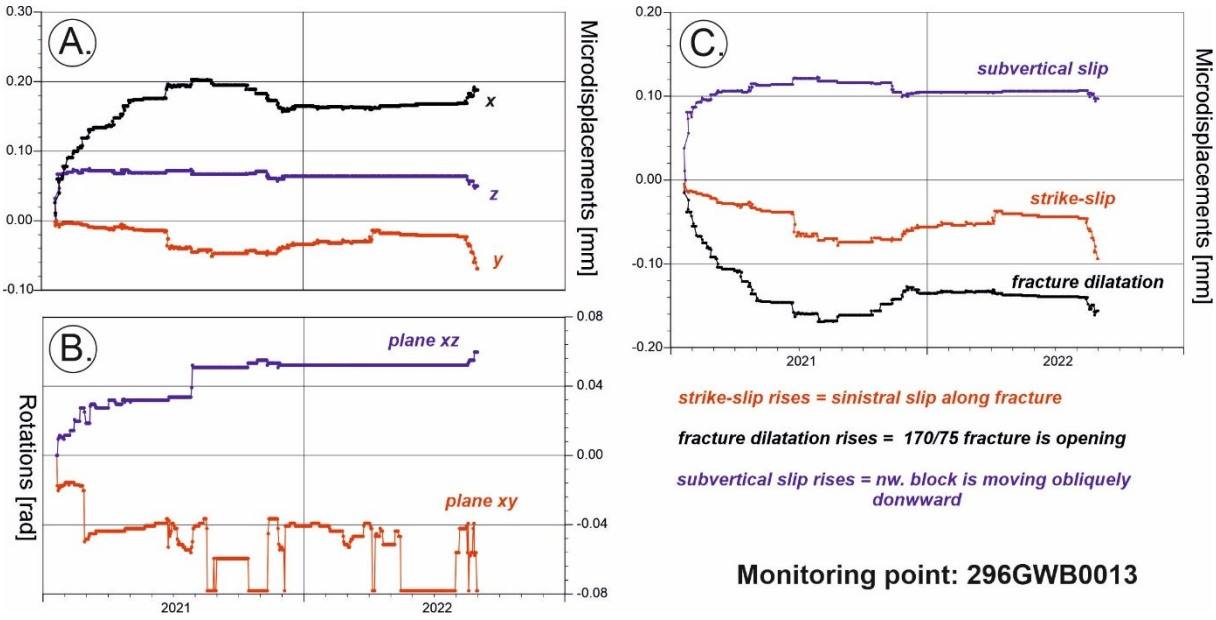

Fig. 22 Extensometric monitoring results at 296GWB0013 site.

4.13 The 296GWB0014 Monitoring Point

All movement components on this brittle structure show a trend which can be accelerated or temporarily attenuated (Fig. 23, Graph C). Before 8 May 2021 activity was identified in all components, which ceased on that day. This period of inactivity continued and was only interrupted by a short pressure event with right-lateral slip, closing the brittle structure and reverse slip of the NE block on 17–25 June 2021. After this event, the movements ceased again. We observed that movements ceased from 26 June 2021 for instance also at points 296GWB0013, 296GWB0008, 296GWB0005 and 296GWB0004. The present data already allow us to assume that the slips will be affected by thermal dilatation of the massif. This monitoring site is the closest to the pit, and therefore also to the most significant changes in temperature related to the ventilation of the underground work. The relation to the air temperature (Vylamová et al. 2020) is also documented in Fig. 24, where the monitored X-axis (parallel to the gallery direction) copies the average air temperature obtained at the point VrK-1. The Pearson correlation coefficient r = 0.74 indicates a strong correlation. The estimated value of the seasonal amplitude in the X component will be approximately 0.05 mm. However, monitoring will have to continue here for at least two years in order to distinguish seasonal cycles from actual fault movements caused by endogenous processes.

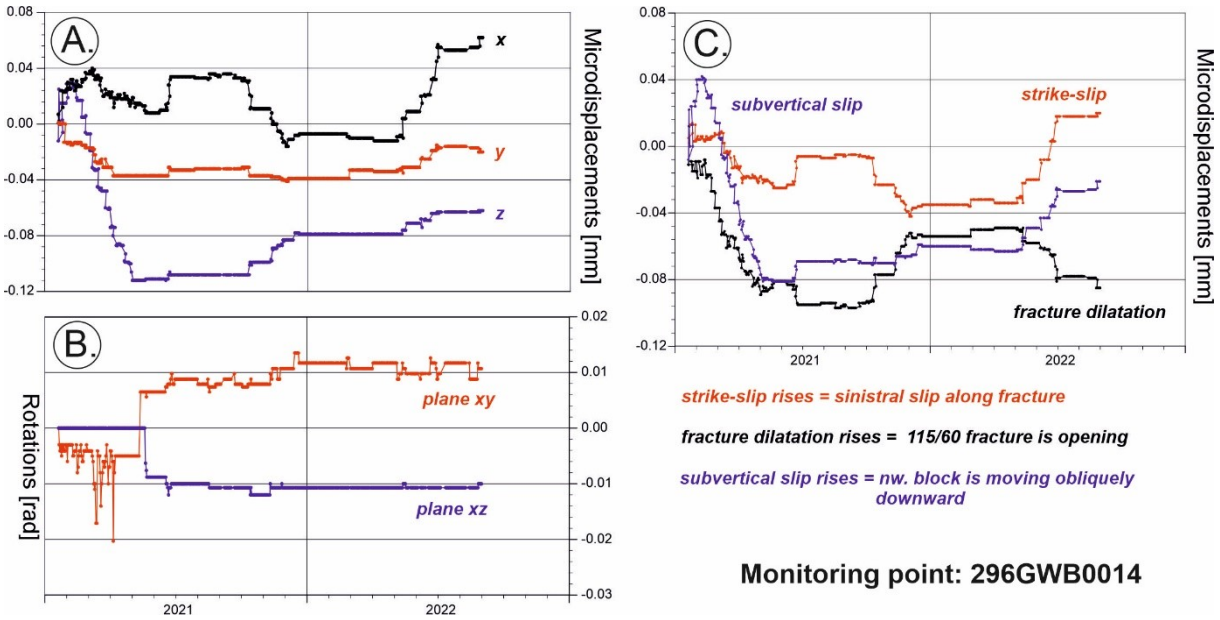

Fig. 23 Extensometric monitoring results at 296GWB0014 site.

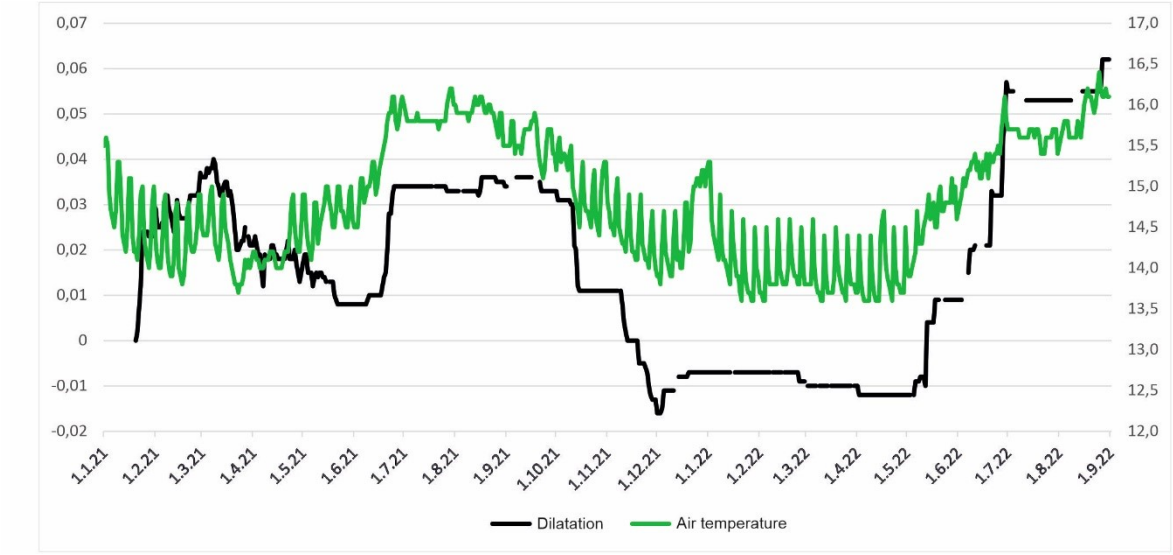

Fig. 24 Air temperature (Vylamová et al. 2020) versus displacements at 296GWB0014 site.

5 Numerical Model

The simulation was done in Plaxis 3D VIP finite element analysis SW. Detailed documentation for the software is available at https://communities.bentley.com/products/geotech-analysis/w/wiki/46137/manuals---plaxis. Elastic deformation analysis was carried out, as part of which the brittle structures were incorporated into the model as weak rocks (with significantly lower deformation parameters than those characteristic for the rock massif). As part of the solution, a “quasi-2D” model was prepared. It is a 3D horizontal section through the Bukov URF at approximately -563.5 m and -546.5 m (for the model image, see Fig. 25). The reason for using the 3D modelling tool, instead of 2D plane-strain analysis, is the possibility to include the influence of driving the galleries in the Bukov URF on the state of stress in the rock massif.

After generating the initial state of stress and simulating the driving of the underground galleries, the computation attempted a back-analysis of the measured movements on discontinuities by applying horizontal pressures on each block. The results yield information on the state of stress and pressure in the area, and the interpretation of disturbances by tectonic lines.

As only a 2D solution has been studied from the viewpoint of disturbance, only horizontal movements on discontinuities have been interpreted; the method does not allow the interpretation of vertical movements. To interpret them, it would be necessary to prepare a full 3D model, which is outside the scope of this task.

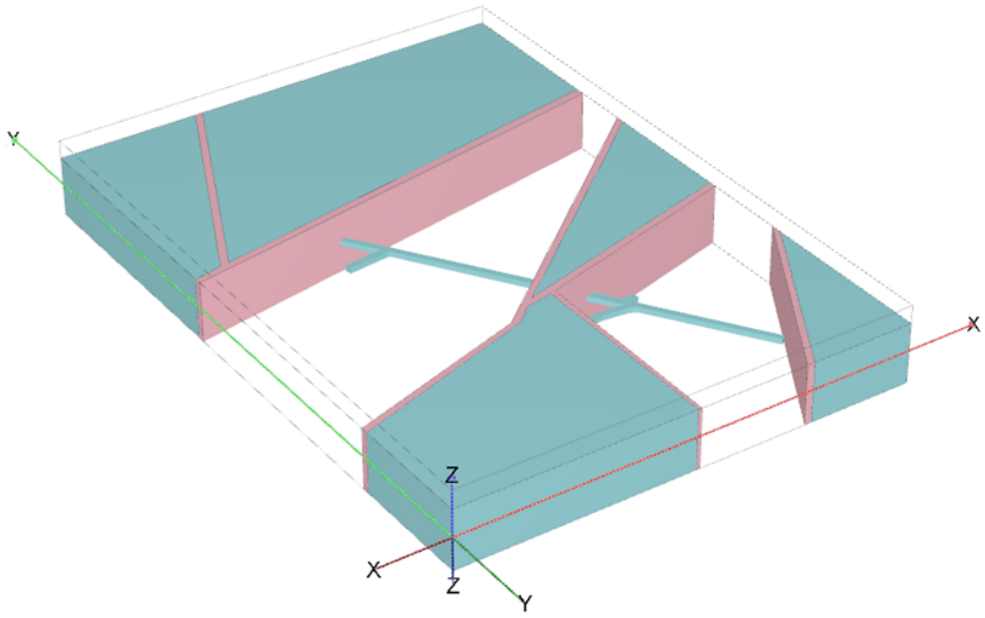

Fig. 25 *Geometry of the model adopted in simulations.*

5.1 Model Geometry

The simulated area was 250 x 350 m in size, and its orientation according to the geographical coordinate system was selected, while the area was extended to cover not merely the closest vicinity of the URF galleries. Fig. 26 displays the entire simulated area in combination with the map of the Bukov URF in the standard extent and rotation.

The area was divided into a system of blocks and discontinuities. Only those discontinuities were defined where more significant horizontal movements were measured, i.e., the selection does not follow the entire thickness and character of the discontinuities (see Chapters 2 and 3 hereof), as some more significant discontinuities do not indicate a more significant movement and, on the contrary, on some other discontinuities which are not seen as significant the movements are not negligible.

The course of discontinuities was also simplified to linear (with exceptions) as necessary to maintain the geometrical compatibility of the task. The course of discontinuities on the area borders where no up-to-date data are available is therefore only approximate. The blocks were separated with direct vertical lines in the quasi-2D solution. The full 3D solution, in which inclined lines would be used for interpreting vertical movements, would require a greater vertical extent of the area; however, this was not considered for this task, in accordance with the contract.

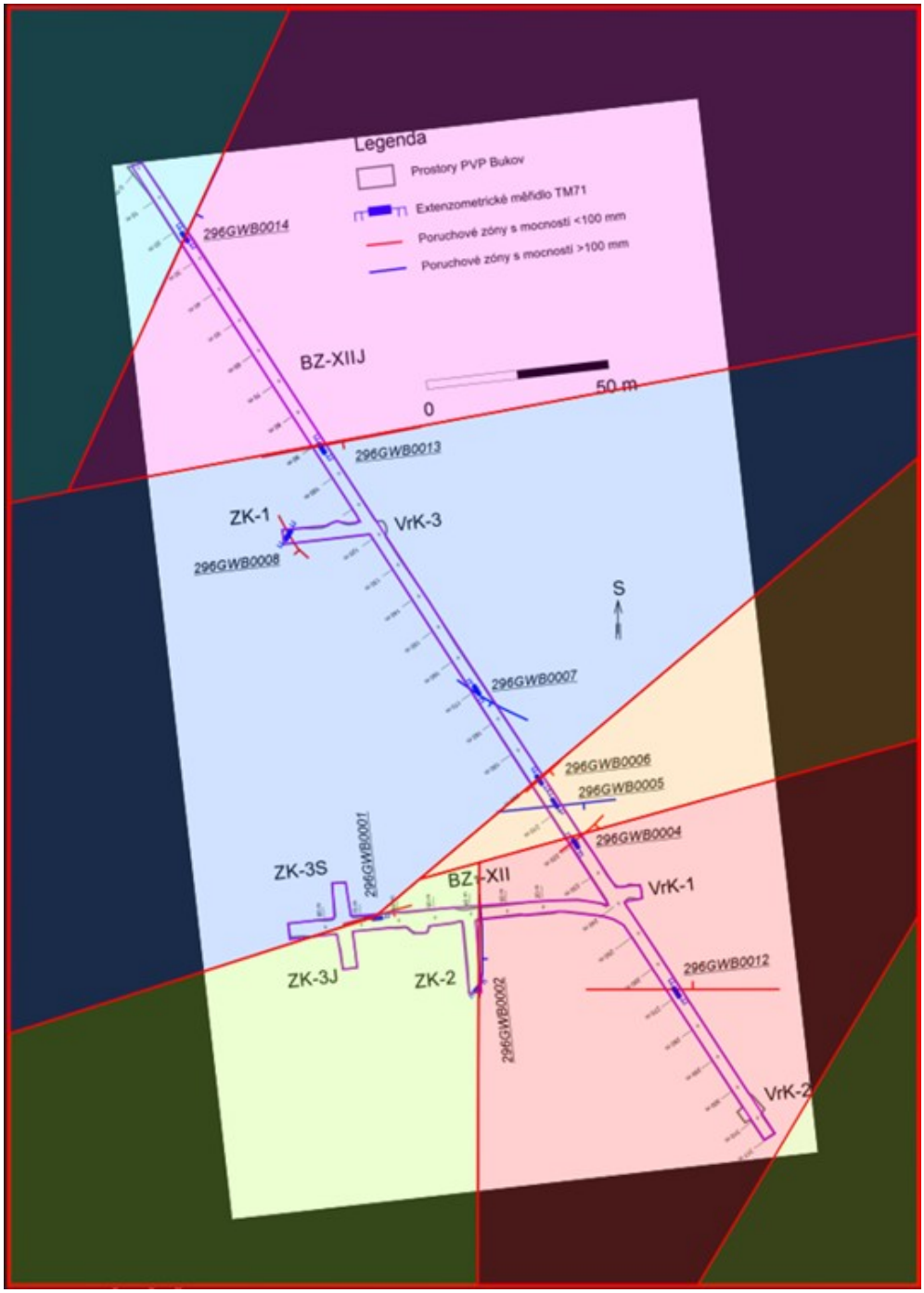

Fig. 26 Simulated area (external borders of the image) shown together with rotated the Bukov URF map for North-South orientation, including separation into quasi-homogeneous blocks.

The driving of open underground spaces for the laboratory was considered for the solution, too. The Geometry of the URF is given in Fig. 26, and the whole model assumes an area overlapping ±15 m over and below the URF level. The Bukov URF is simplified here so that 3 m high vertical walls of the underground work are assumed, making up the total vertical height of the model of 33 m (Fig. 27).

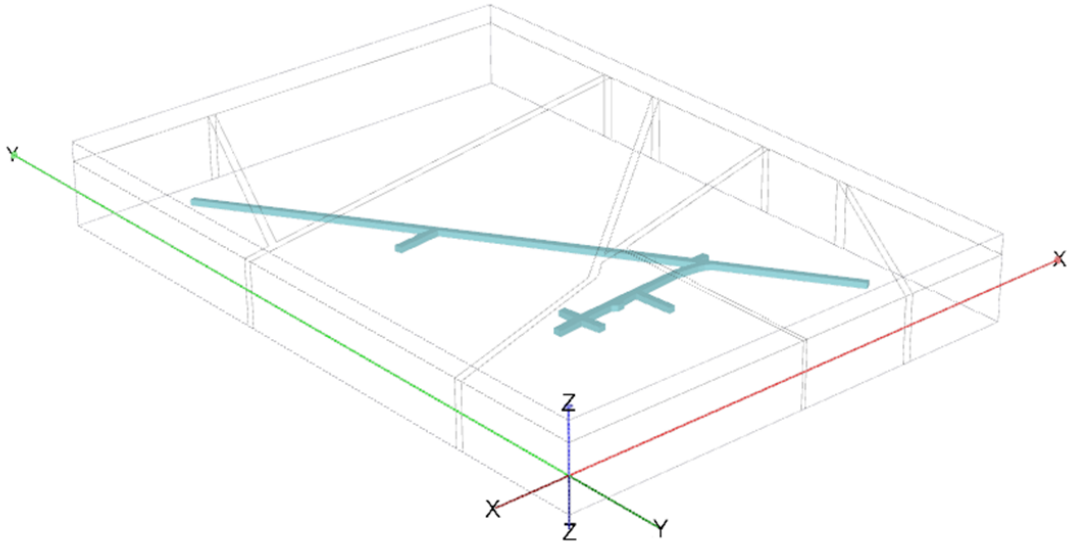

Fig. 27 Adopted geometry of the Bukov URF within the quasi-2D model.

For the geometry so defined, a mesh was generated for the finite element method. The mesh contains 22,242 10-node elements and 33,798 nodes (see Fig. 28).

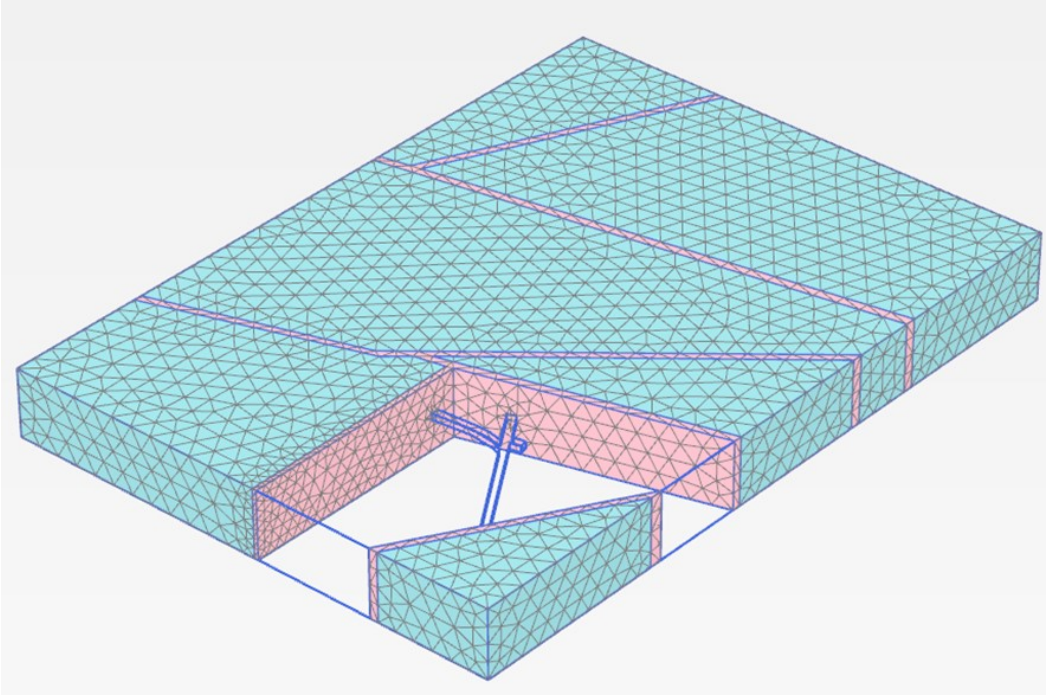

Fig. 28 Finite element mesh used in the models.

5.2 Computation Process and Parameters

An elastic constitutive model was used in the computation, where the parameters of the rock massif were selected in accordance with the results of the geological and geotechnical survey (Souček et al., 2018) and are given in Table 3. The discontinuity parameters were selected so as to represent the apparent weakness zones of the massif: their rigidity was considered as a 1/1000 multiple of the massif's rigidity.

Table 3 Parameters of rock massif and of discontinuities. E represents Young modulus, v Poisson ratio and ρ density.

	E [GPa]	v	ρ [kg/m^3]
Rock massif	50	0,15	2850
Discontinuities	0,05	0,15	2850

The model was processed in the following phases, the geometry of which is given in Fig. 29–Fig. 33:

1. In the first phase (Fig. 29), the geostatic state of stress was initialised: the effects of the geostatic load were simulated, giving isotropic pressure of 15 MPa. Due to the characteristics of the software (initialisation of the initial state using the surface load is impossible), the geostatic load was modelled in order to simplify the geometry as a narrow (10 m thick) rock layer with extreme unit weight of 1500 kN/m3, which is set so as to produce the required isotropic pressure of 15 MPa.

2. In the following phase (Fig. 30), the geostatic load was replaced with equivalent vertical surface load of 15 MN/m^3. This substitution was necessary because the layer made artificially for the state of stress initialisation must not subsequently stabilise movement on discontinuities.

3. In the third phase, discontinuities were activated by replacing the rock material with discontinuity material. As can be seen in Fig. 31, although they represent planar geometrical entities with a negligible width from the viewpoint of the overall dimensions of this task, discontinuities were simplified for the purposes of the model and extended so that their width could represent one element in the finite element method (approx. 3 m).

4. In phase 4, the driving of the URF was simulated. As the solution of this task is not aimed at geotechnical analysis of the excavation, the entire tunnel was removed in a single phase, and gradual driving was therefore not simulated. Despite this approximation, the model indicates a significant change in state of stress in the proximity of the tunnels (see also Fig. 34).

5. In the 5th and last phase, horizontal pressures were applied for the purposes of the displacement of the massif on discontinuities. Lower or higher load than the average 15 MPa leads to displacements on the boundary between blocks. A load within the range of 5 to 30 MPa was applied (compared to the original value of 15 MPa), see various views in Fig. 33 where load is marked with blue arrows. To obtain a statically definite solution, some blocks were selected as immovable in the strike direction on the boundary with free deformation in a longitudinal direction (see green supports in Fig. 33) – relative deformation in the model was then simulated against them.

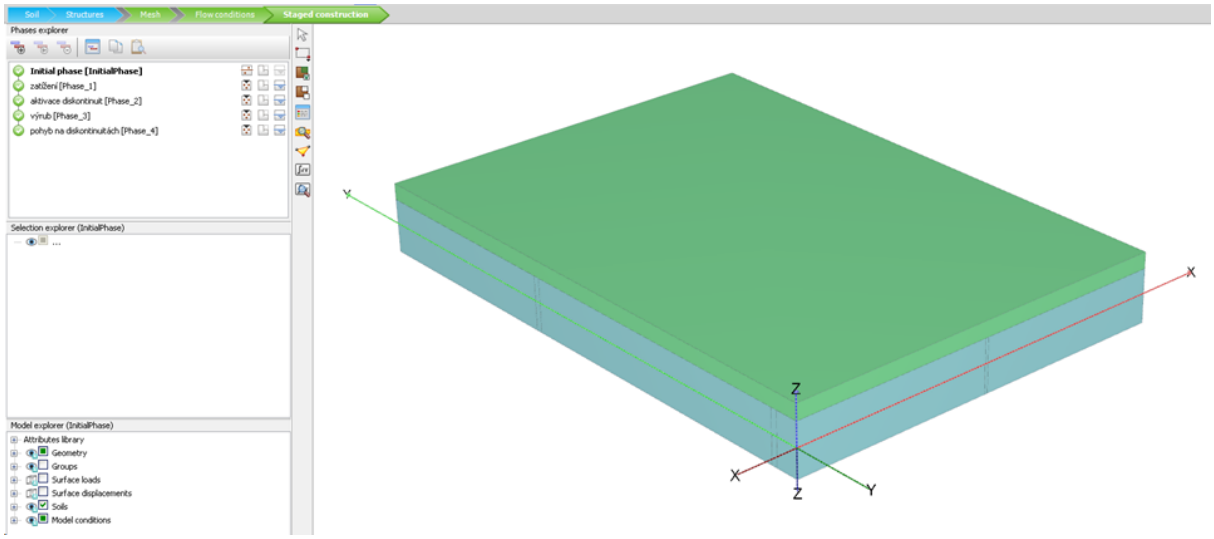

Fig. 29 Geometry of phase 1

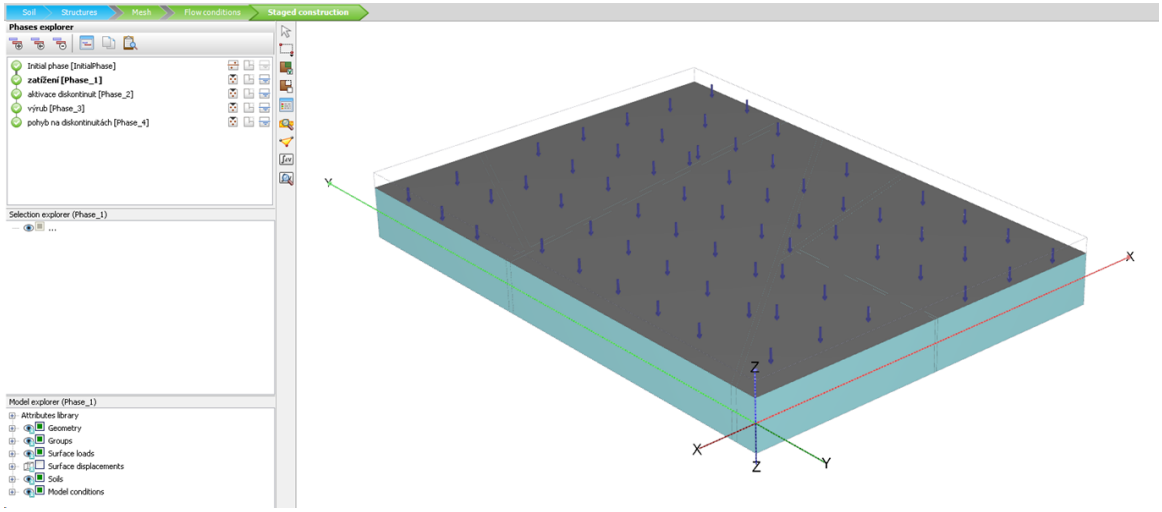

Fig. 30 Geometry of phase 2

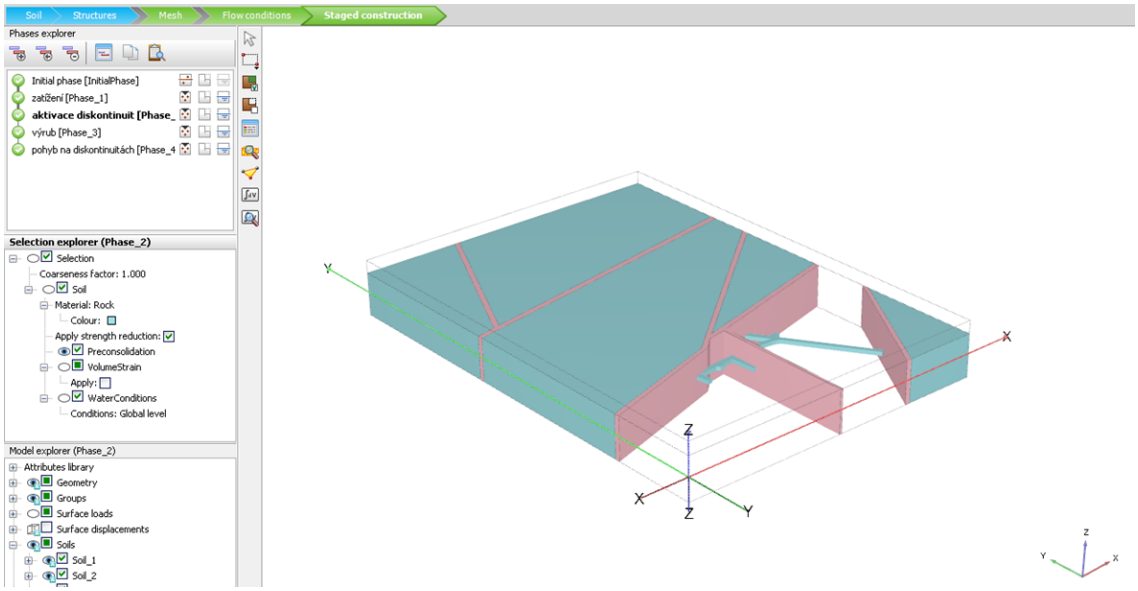

Fig. 31 Geometry of phase 3

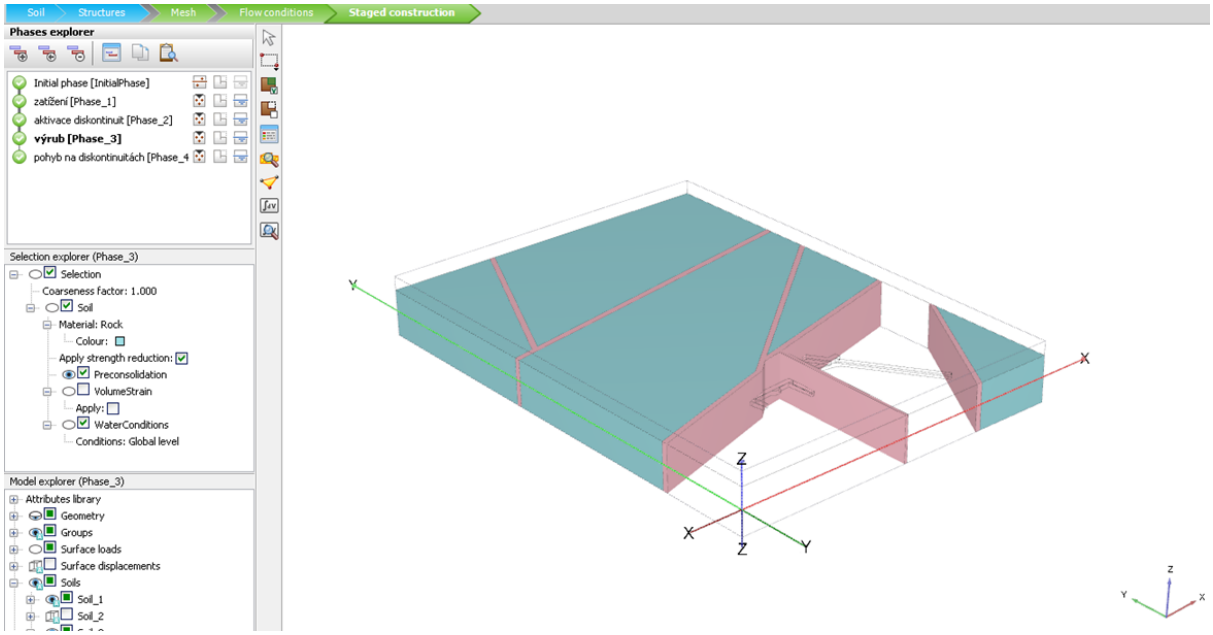

Fig. 32 Geometry of phase 4

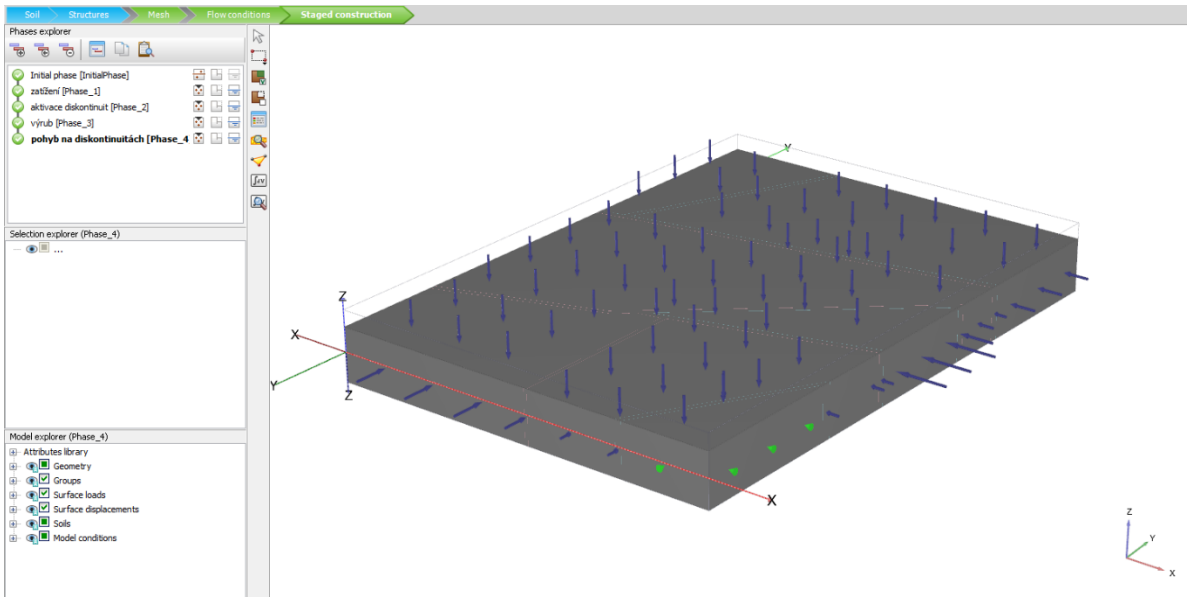

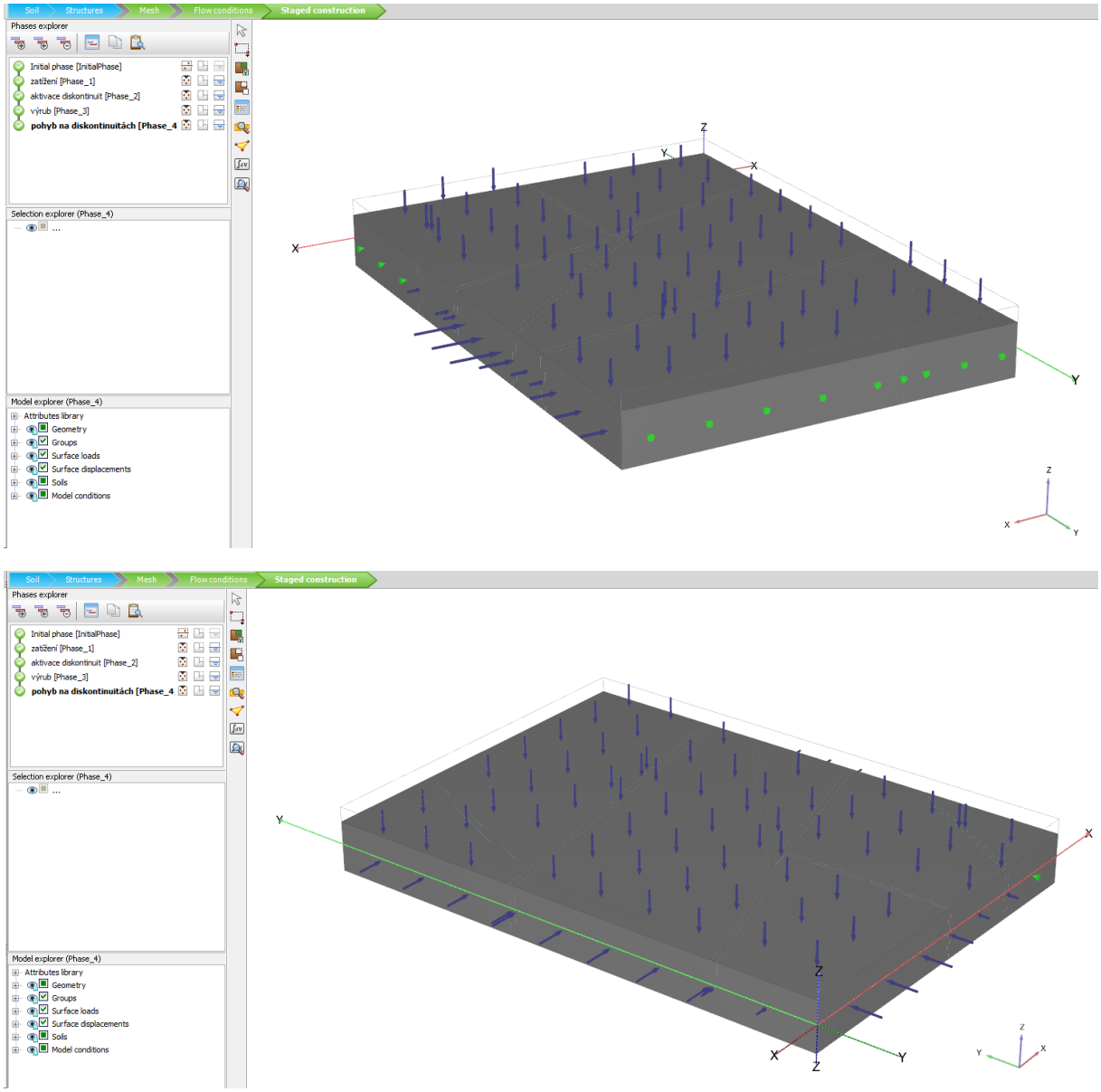

Fig. 33 Geometry of phase 5, views from different directions

5.3 Simulation Results

5.3.1 Comprehensive Summary of Results

Fig. 34 is an illustration of the change in state of stress caused by the tunnel excavation used in phase 4 of the simulation. It is apparent that there were major changes against the initial geostatic stress. A detailed description of state of stress falls outside the scope of this task, as gradual driving of the tunnel would have to be simulated to determine it, a relevant material model reflecting the plastic behaviour of the massif would have to be used, and a significantly finer mesh of finite elements around the tunnel would have to be defined.

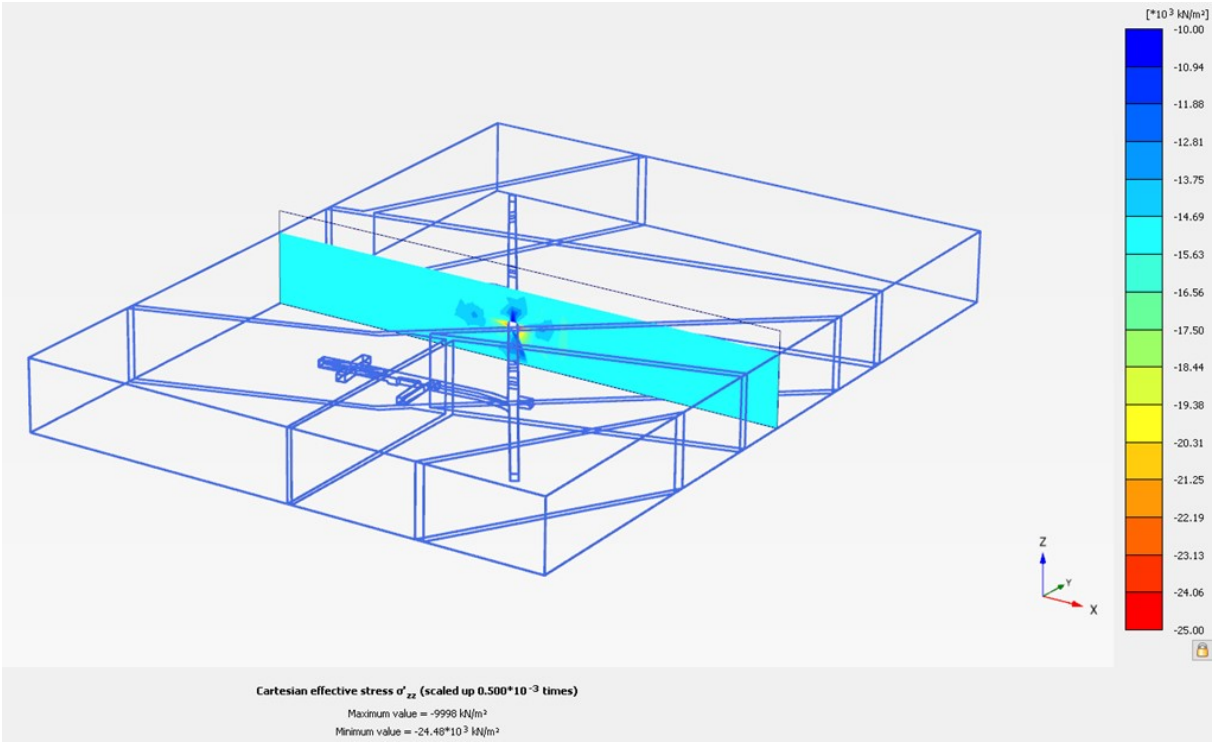

Fig. 34 Change of stress due to tunnel excavation

The relative movements of quasi-homogeneous blocks and the change in state of stress of the massif caused by geological processes are the main outputs of the model. The results are gradually presented in the form of imagery of displacements by means of the deformed finite elements mesh (with 12,000 times magnification of deformations for better interpretation). Further, using contour maps, values are displayed of two strike-slip components, and the total displacement also marked with vectors. The total state of stress is presented in contour maps of strike components of the tensor of stress in two horizontal directions (Fig. 35 - Fig. 41).

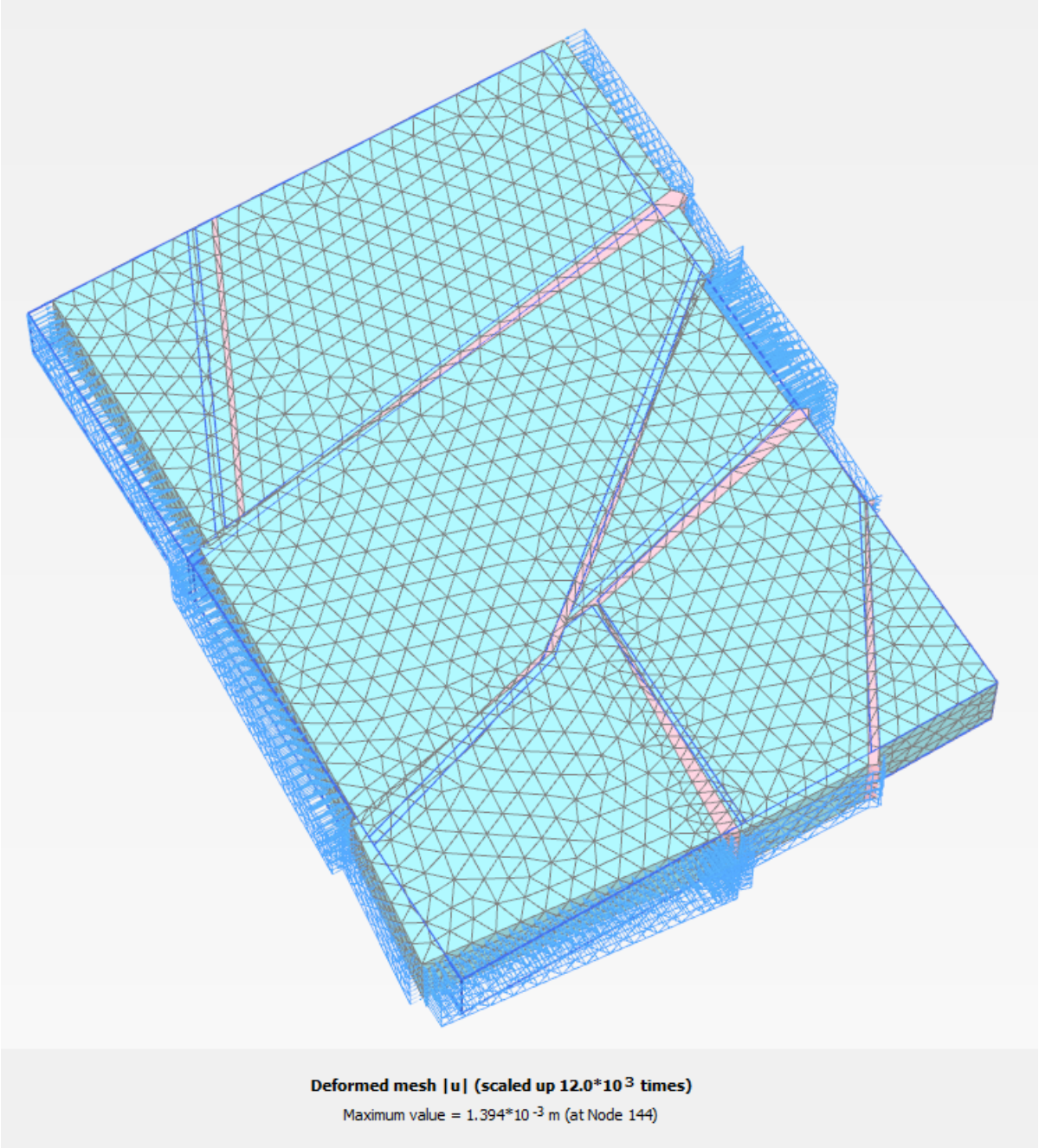

Fig. 35 Simulation results: deformed mesh (12000x exaggerated)

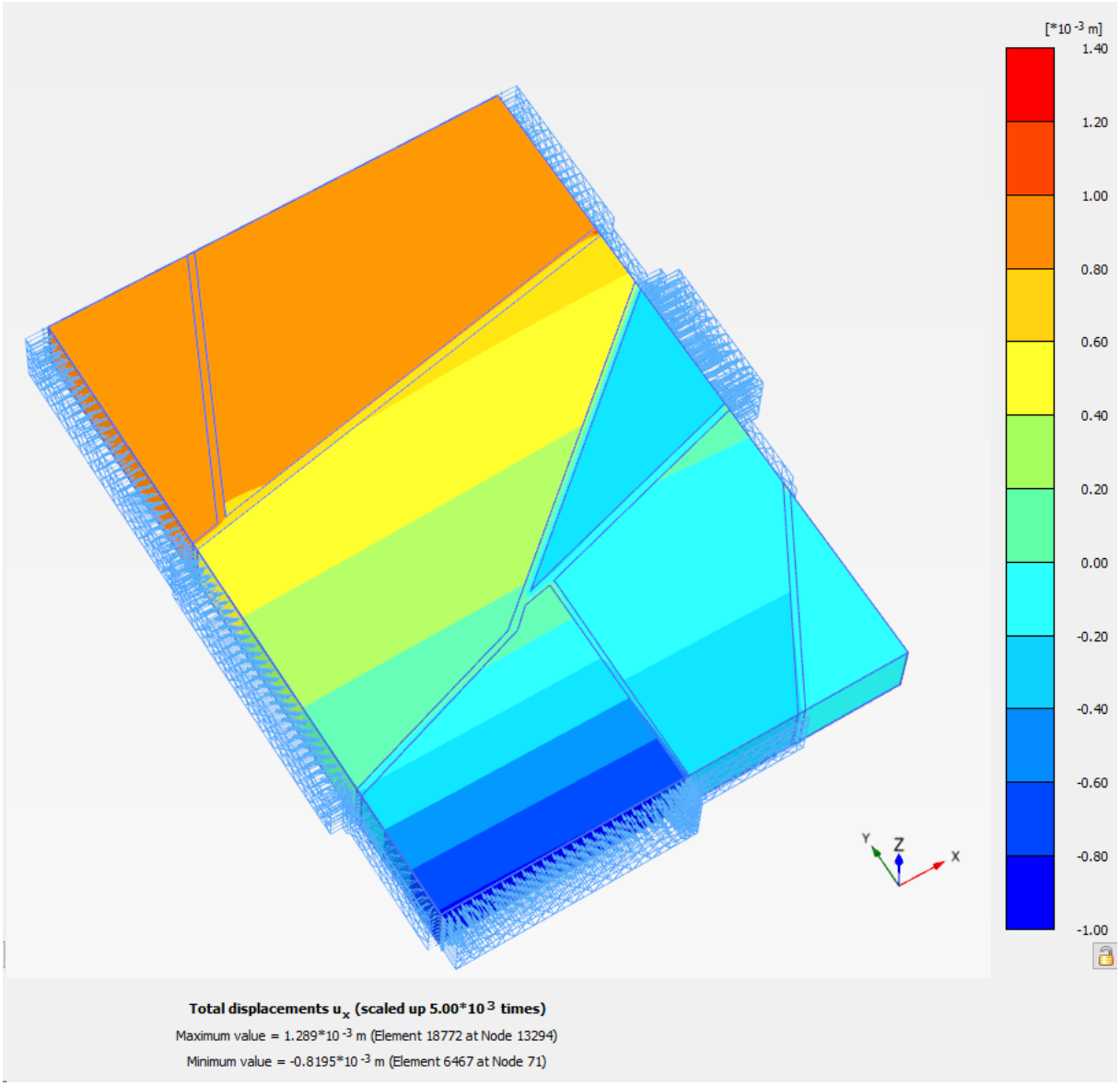

Fig. 36 Simulation results: horizontal displacement, direction x

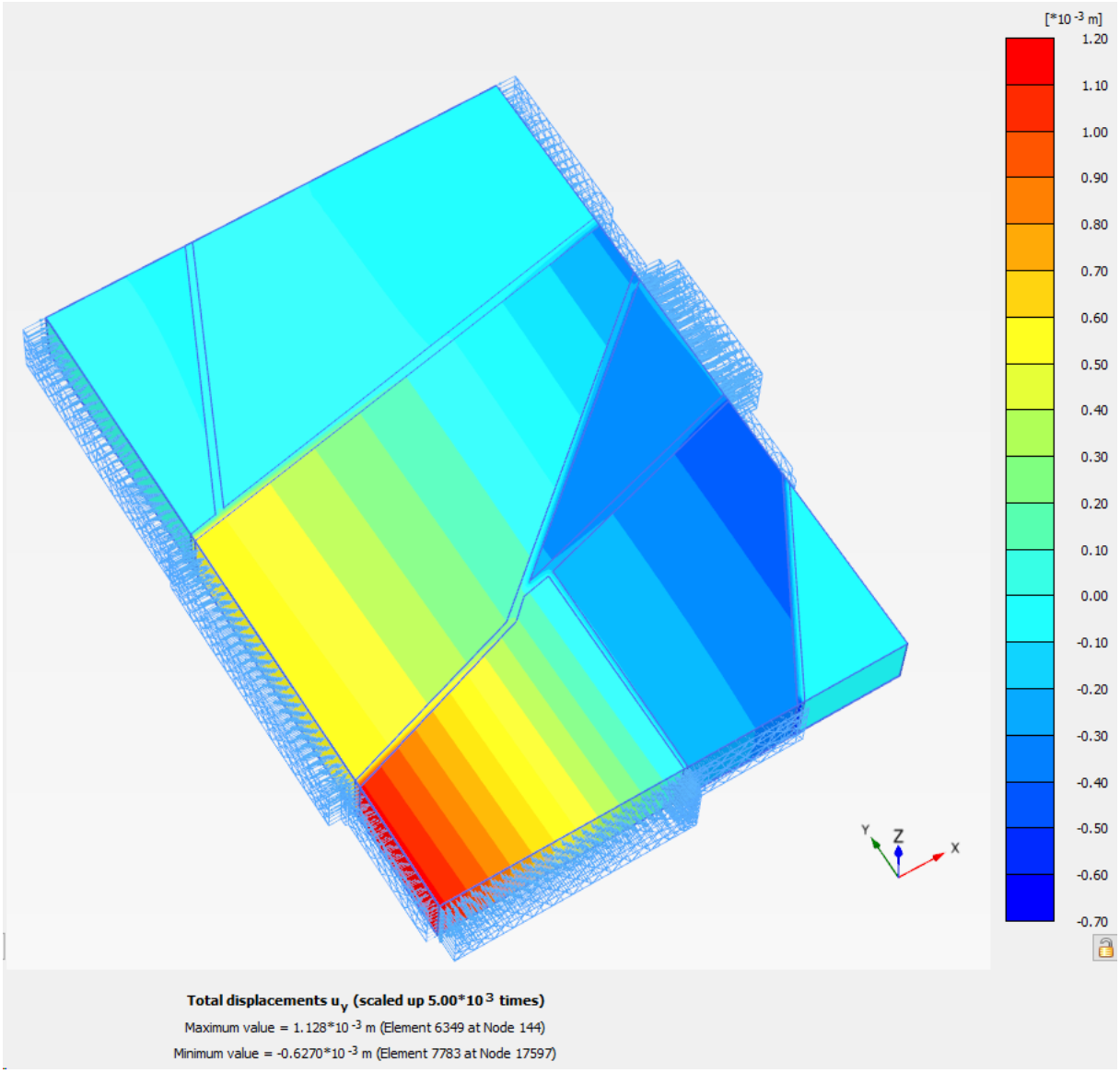

Fig. 37 Simulation results: horizontal displacement, direction y

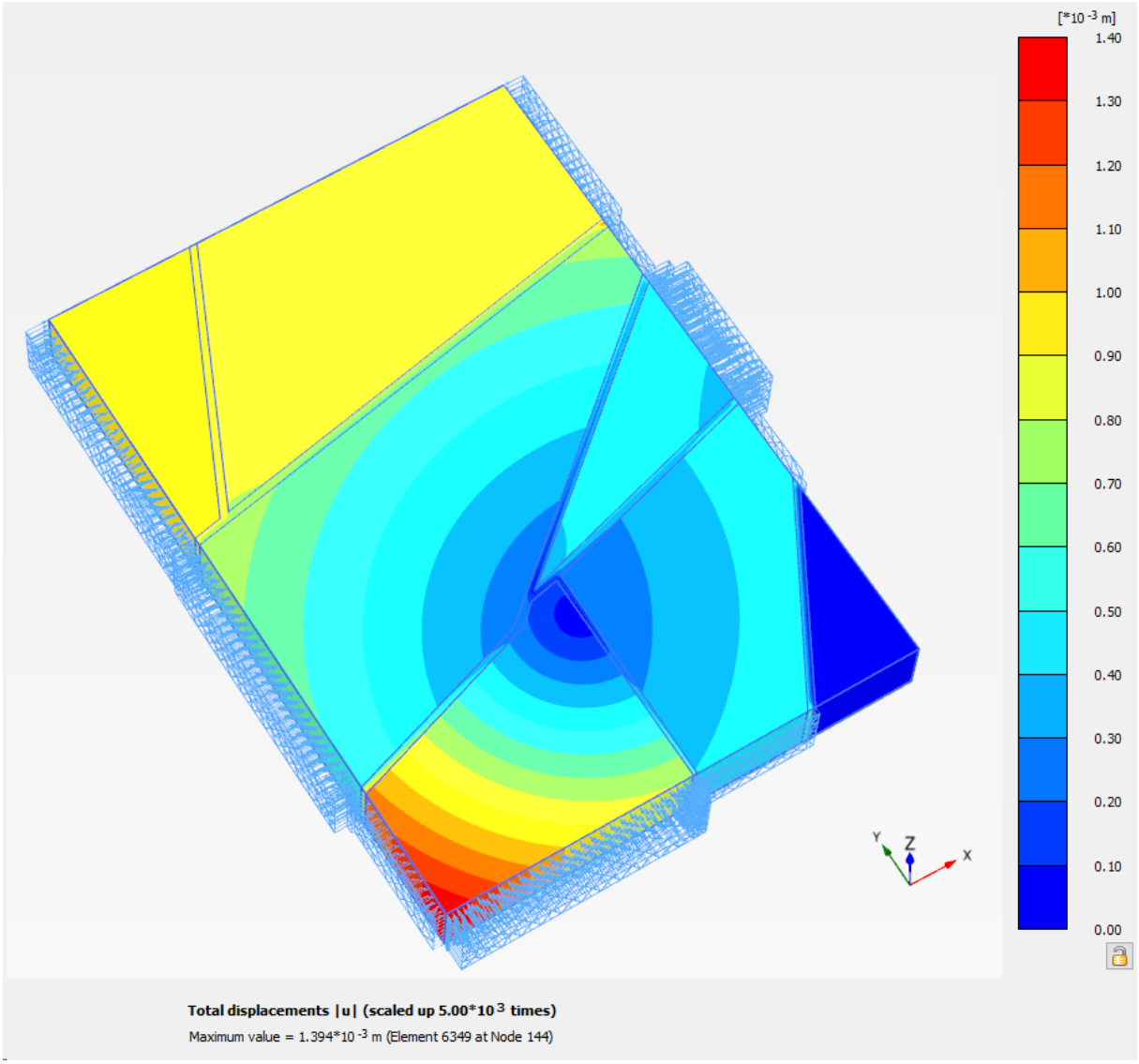

Fig. 38 Simulation results: horizontal displacement, total magnitude. The result indicates clear rotation of South-West block.

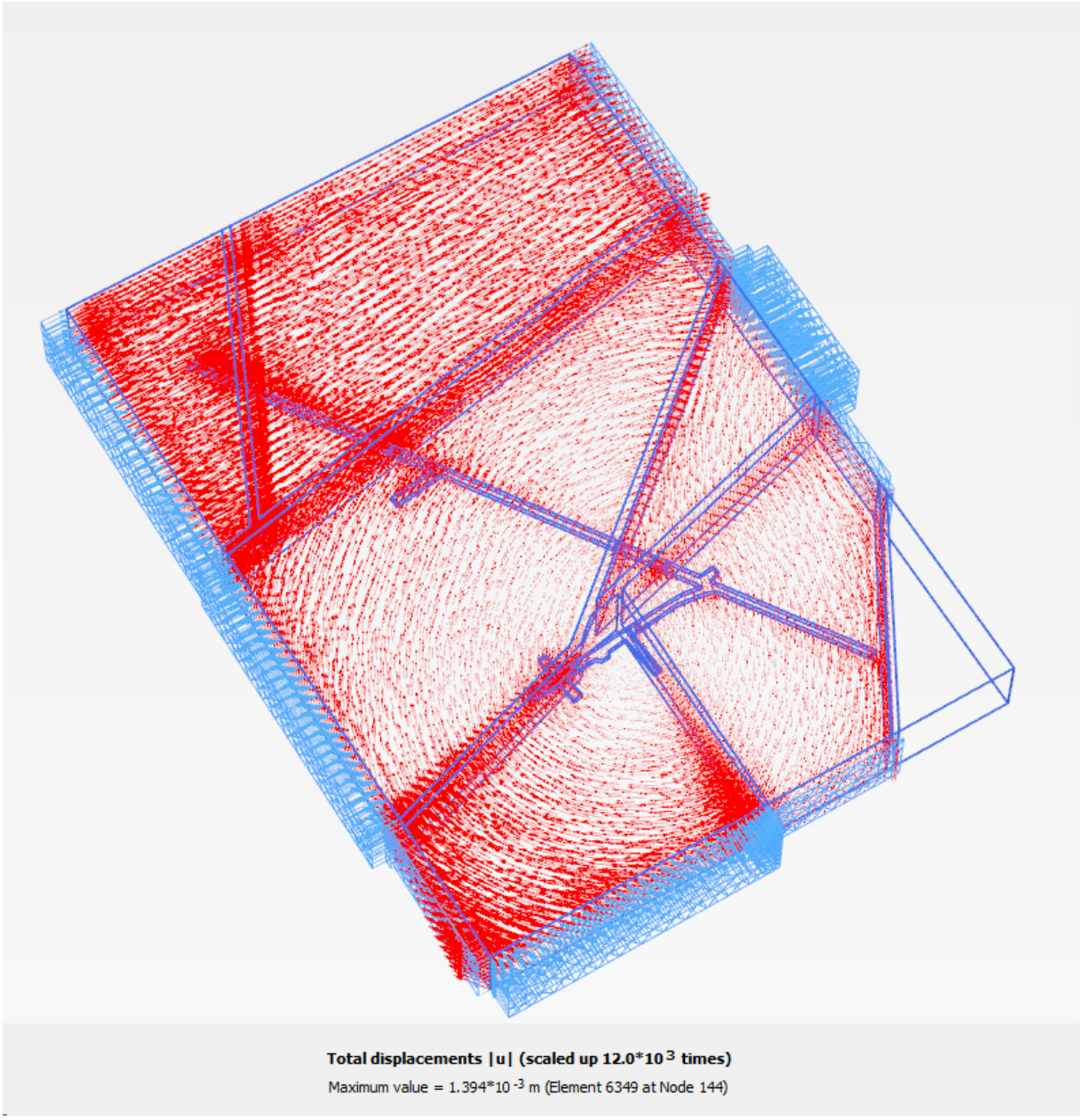

Fig. 39 Simulation results: displacement vectors (length multiplied 12000x). The result indicates clear rotation of South-West block.

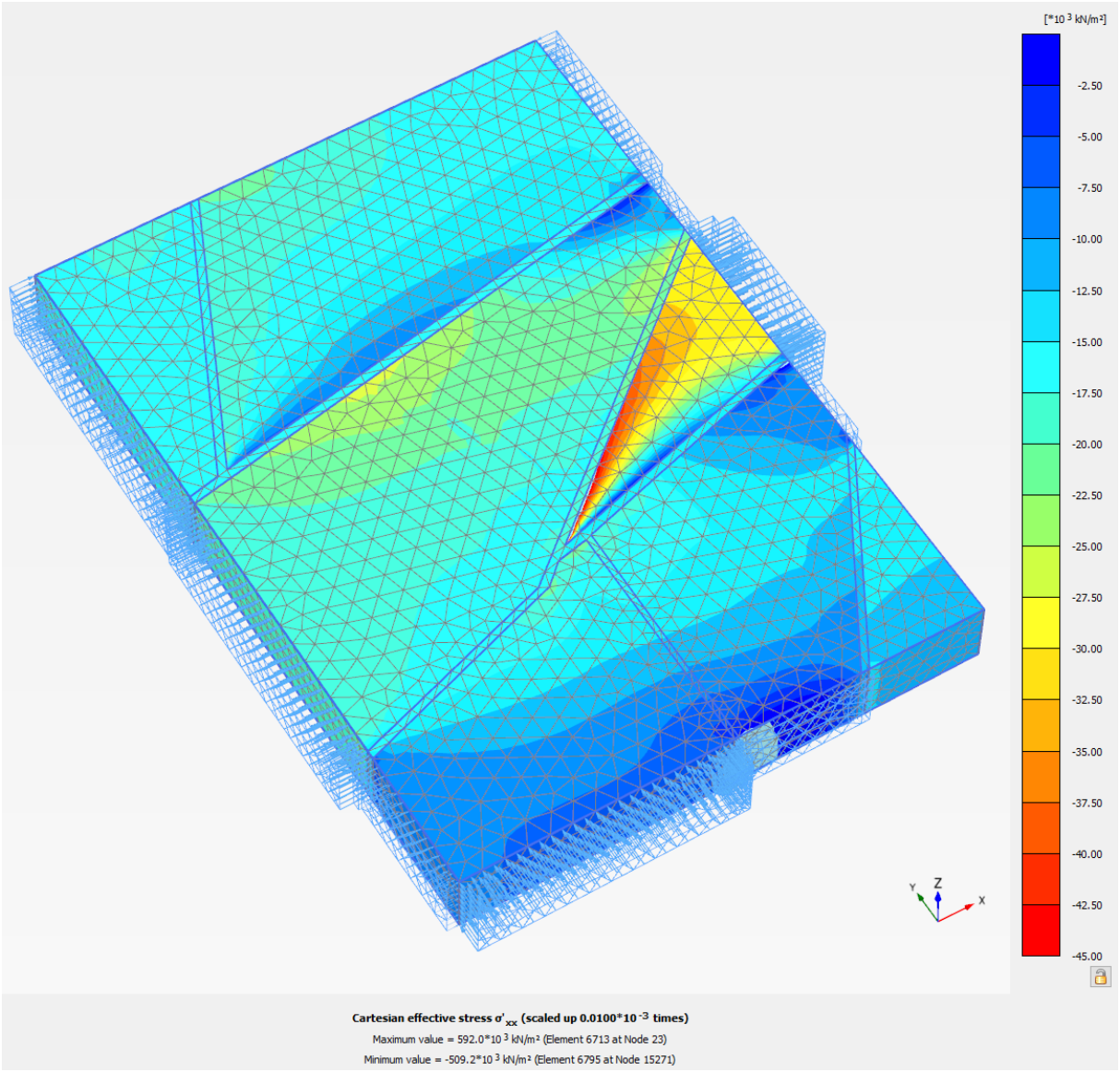

Fig. 40 Values of stress, horizontal normal component of the stress tensor in x-direction.

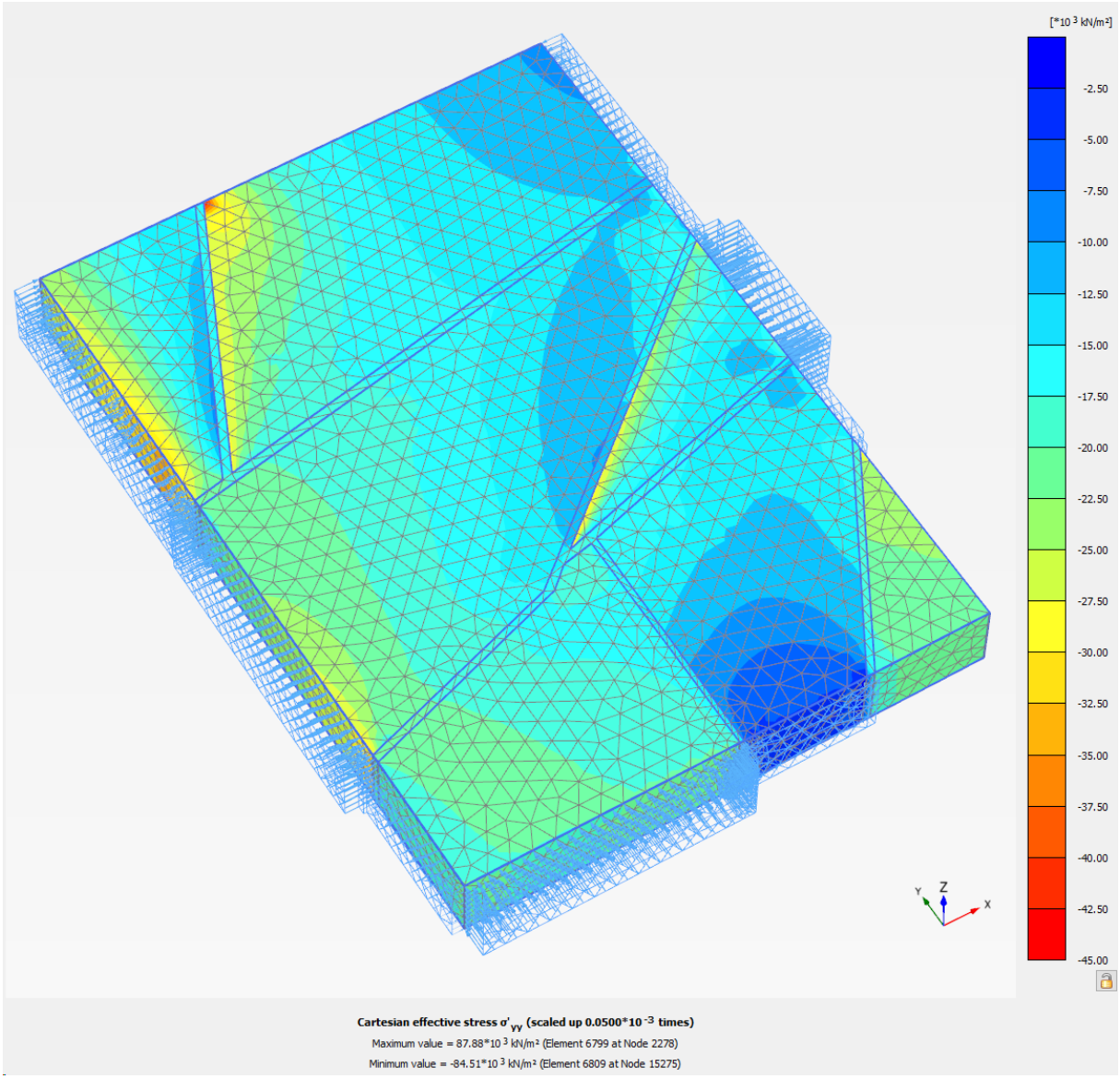

Fig. 41 Values of stress, horizontal normal component of the stress tensor in y-direction.

5.3.2 Comparison of Results with the Measured Quantities

5.3.2.1 Deformations on Discontinuities

The qualitative comparison between the measured deformations and the relative movement of the rock blocks is displayed in Fig. 42. It is apparent in the figure that the relative movements on the main discontinuities are presented correctly.

The overall size of deformations is apparent from Fig. 36 to Fig. 38. The relative movements on blocks are around 0.5 mm, which is the upper limit of the measured displacements on the discontinuities with the greatest movement. The comprehensive character of the optimisation task allowed us to find settings that give the correct relative movement of blocks (Fig. 42); an accurate forecast of the measured values, however, is beyond the capacity of the method used, which strives to express the general behaviour of the massif.

It must also be mentioned that the measurements are influenced by a significant seasonal component (which was not simulated in the model), and the time span of the measurements is relatively limited to obtain information on long-term trends.

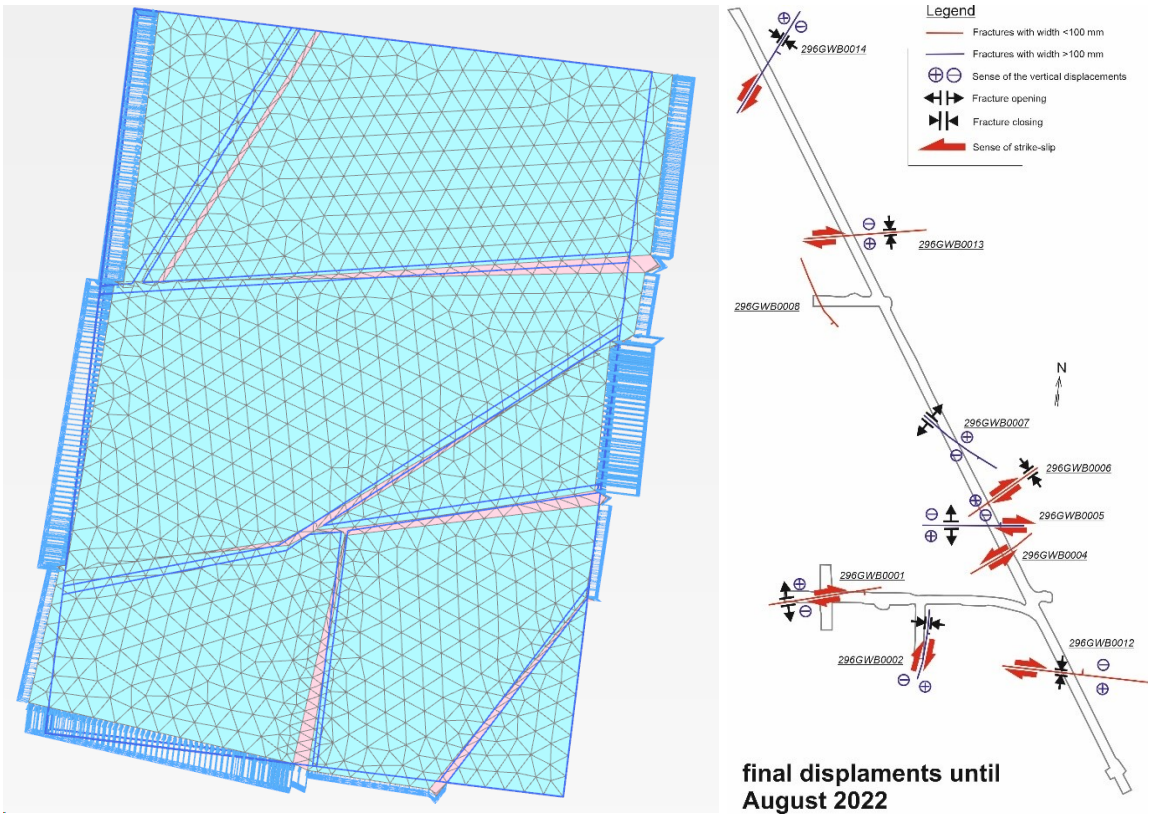

Fig. 42 Qualitative comparison of measured displacements with relative movement of rock blocks

5.3.2.2 State of Stress

The predicted stress in the massif is displayed in Fig. 40 and Fig. 41. The predicted values correspond to the load values on the area boundaries as applied in back-analysis to obtain the correct relative movements of individual rock blocks. The value of stress lies between 5 MPa and 30 MPa, and in extreme cases it may be up to 45 MPa in areas of concentrated stress on the edges and sides of the blocks. The results are comparable not only in orders of magnitude, but also in numeric values with stress measurements made by various methods as presented in the report by Souček et al. (2018), see Table 4. The values of vertical stress are close to the anticipated value of 15 MPa and have lower variance. The values of horizontal stress show a greater variance than those of vertical stress and range from 7 MPa to 38 MPa, which is highly consistent with the predicted values obtained from the numeric model, i.e., 5–45 MPa.

Table 4 Results of rock massif stress measurements using various methods (taken from Souček et al., 2018)

Metoda měření stavu HM	Lokalizace/ č. vrtu	Vzdálenost měření od důlního díla [m]	S_v [MPa]	S_H [MPa]	OH [°]	S_h [MPa]
HF	GS1/ S-8	15 - 30	-16,5*	-17 – -31	358 - 23	-10 – -14
HF	GS3/ S-18	25 - 41	-16,5* (-15,3** přímé měření)	-29 – -38	28 - 45	-12 – -19
CCBO*	GS1/ S-5	14,5 (půdorysná vzdálenost 7,5)	-5,7	-8,1	77	-5,9
CCBO	GS2/S-9	7,4	-7,0	-15,4	16	-2,9
CCBO	GS2/S-11	22,6	-10,6	-10,1	16	-7,2
CCBO	GS2/S-12	6,7	-13,9	-11,2	26	-5,3
CCBO	GS2/S-13	11,6	-14,8	-14,6	144	-5,1
CCBO	GS2/S-21	20	-7,9	-7,0	146	-4,9
INVGEM	KS2	--	-16,5*	-19.8	30 -87***	-11,5
INVGEM	KS3 a KS4	--	-16,5*	-38,0	41	-4,6

6 Conclusions

6.1 Measurements in the Bukov URF and in the Rožná Mine

The measurement of movements on brittle structures which took place at the Bukov URF from the end of 2019 to August 2022 can already prove movement trends for some locations within the facility. These trends are measured in hundredths to thousandths of a mm/yr. At point 296GWB0001 we observed a trend of 0.1026 mm/yr in subvertical slip and a right-lateral strike-slip of 0.026 mm/yr; right-lateral strike-slip at point 296GWB0002 with a trend of 0.091 mm/yr, and closing of the fault of 0.06 mm/yr; a strike-slip at point 296GWB0004 with a trend of 0.112 mm/yr; dilatation at point 296GWB0004 with a trend of 0.17 mm/yr; strike-slip at point 296GWB0006 with a trend of 0.03 mm/yr and closing of the fault at 0.04 mm/yr; a subvertical slip at point 296GWB0007 with a trend of 0.09 mm/yr and closing of the fault at 0.07 mm/yr. The measurements available so far have therefore yielded displacement trends for the entire Bukov URF up to 0.1 mm per year.

At three new points, namely 296GWB0012, 296GWB001 and 296GWB0014, no trends can be defined due to the short measurement period, which commenced at the beginning of 2021. However, in more than one location the movements were influenced by seasonal components which most probably relate to the thermal dilatation of the massif thanks to exchange of air by ventilation. The amplitude of this seasonal component at point 296GWB0004 is 0.04 mm for subvertical slip and 0.04 mm for crack dilatation; at point 296GWB0005 it is 0.03 mm for crack dilatation; at point 296GWB0006 it is 0.01 mm for crack dilatation and 0.018 mm for strike-slip; at point 296GWB0007 it is 0.05 mm/yr; at point 296GWB0014 it is 0.05 mm for dilatation. The seasonal component is most significant at these points. The values are less than 0.05 mm, and it appears from the values obtained so far that the highest amplitudes are measured in the zones with a width exceeding 1 m. These include faults monitored at points 296GWB0007 and 296GWB0014. Further measurements will prove this hypothesis. The question also remains why the displacements are significantly affected only in the BZ-XIIJ gallery. The temperature curve for the air that should influence the thermal dilatation of the rock massif is the same in galleries ZK-3S and BZ-XIIJ (Fig. 43). In locations outside the BZ-XIIJ gallery, no movements with a seasonal amplitude have been observed, but they were seen on the lower levels of the Rožná mine at points 296GWB0009, 296GWB0010 and 296GWB0011. As the time span of the measurements was short, we were unable to define the amplitude of the seasonal component (see the TZ 526/2020 Report). These points were cancelled after nine months of measurements because of the planned inundation of the lower levels of the mine. Trend movements at the Bukov URF are usually interrupted or combined with accelerated slips which occur during periods of higher tectonic activity. Such a period was observed, for instance, in May/June 2021, when a compression regime was observed on the monitored brittle structures, accompanied by the closing of faults and dip slip of the S, SW and SE blocks in general (Fig. 44). After this active period, there was a period of inactivity which generally started on 26 June 2021. The beginning of the period was observed at points 296GWB0004, 296GWB0005, 296GWB0008, 296GWB0013 and 296GWB0014. Some locations saw an earlier beginning of the period. The aforementioned compression period was in contrast to the extension period (Fig. 44) which we observed in November 2019 / February 2020 (see the TZ 526/2020 Report). Changes in stress and regime are supported, for instance, in Fig. 45, which also clearly indicates the changes in direction of rock block movements.

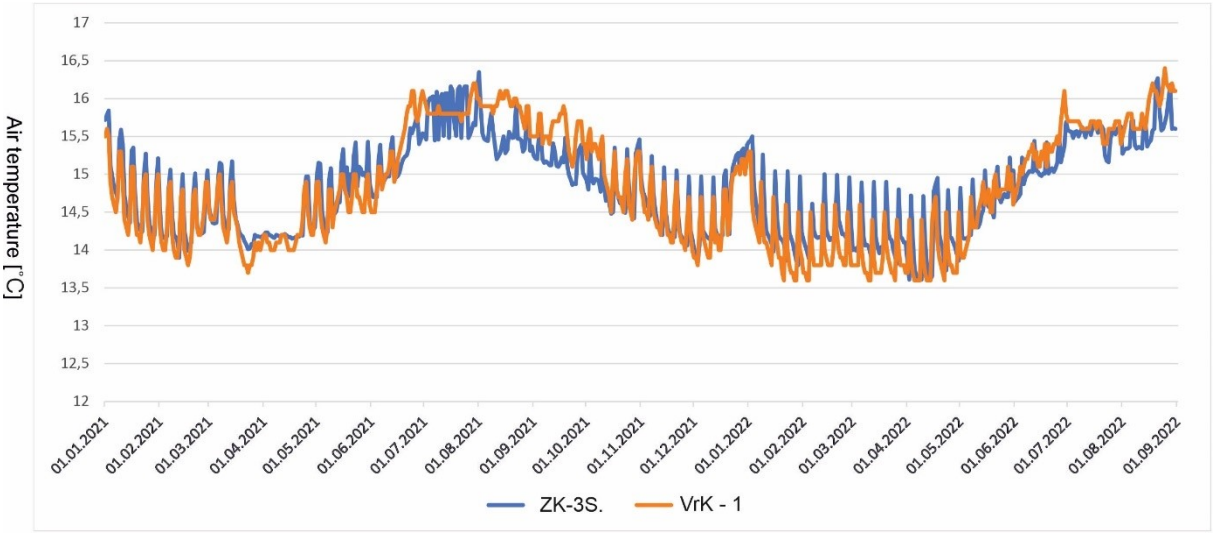

Fig. 43 Air temperature development in the BZ-XIIJ (Vrk-1 point) and the ZK-3S galleries.

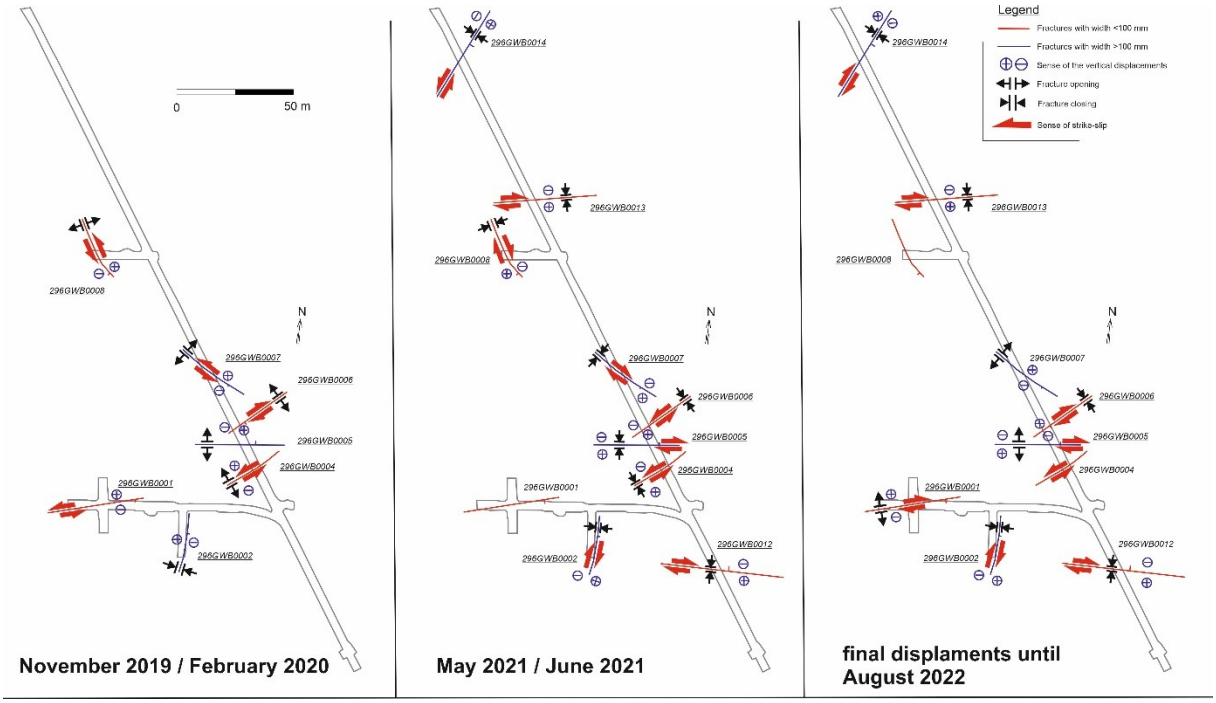

Fig. 44 Schematic illustration of the displacements sense, which developed across monitored brittle structures in Bukov URF during two significant periods (A and B pictures). The first regime could be defined as extensional, second one as compressional. The third picture (C) shows final displacement

across monitored brittle structures during monitoring period (to define long-term trends, we should need longer monitoring time span).

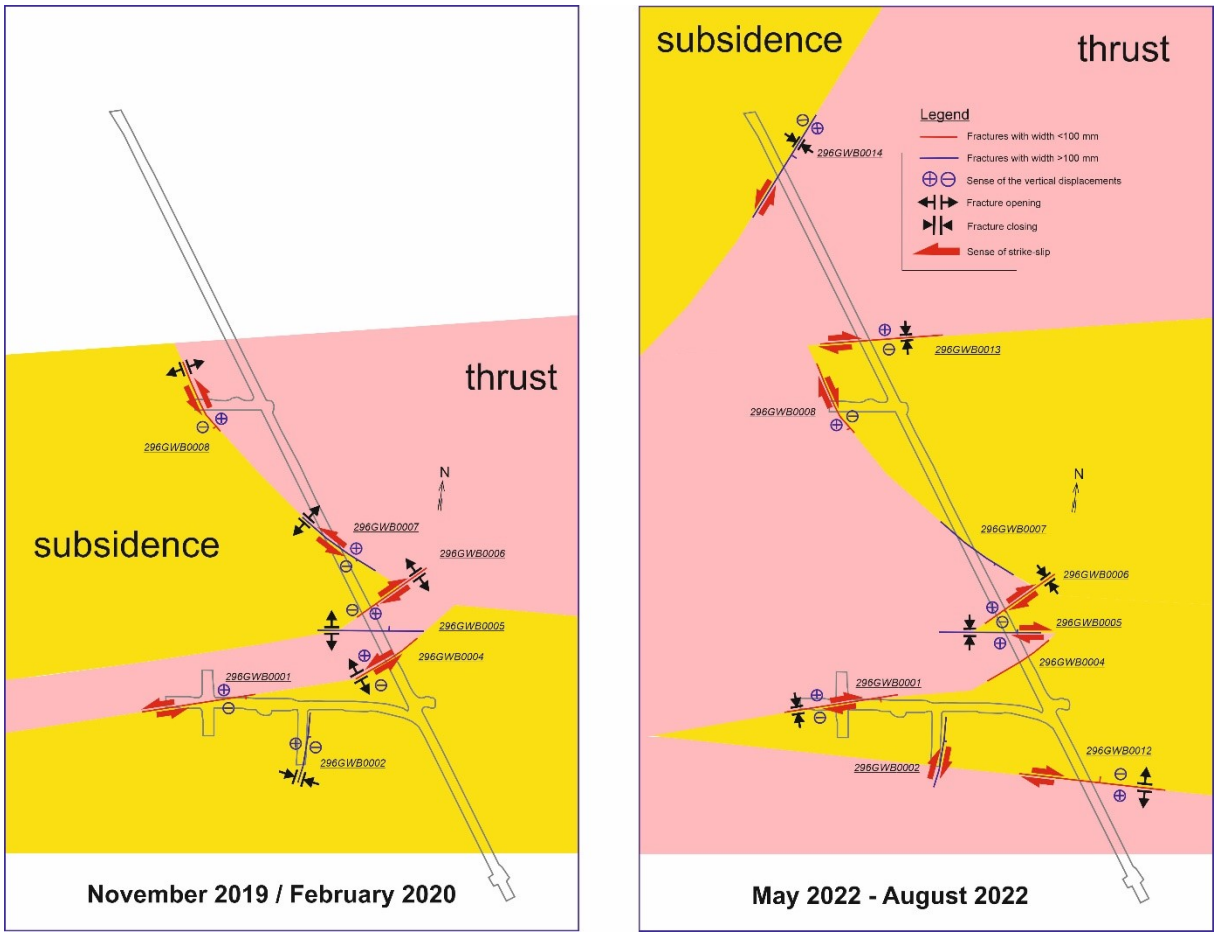

Fig. 45 Vertical displacement comparison of two significant monitoring periods.

6.2 Comparison of Monitoring Results with Other Locations

The displacement trends so far identified, when compared to earlier results from other, especially foreign, locations where extensometric measurements were made using the same method, are low values. For the sake of comparison, we can mention the Krupnik area in Bulgaria, where strike-slip of 2.7 mm/yr was published (Avramova-Tacheva et al., 2007); the average value of strike-slip at the Idrija fault in Slovenia was 0.24 mm/yr and for a short time up to 0.54 mm/yr (Gosar et al., 2011); in the Upper Rhine Plain in Germany, the left-lateral strike-slip along the fault is 0.94 mm/yr (Hoppe et al., 2015). Regarding the results from the same type of monitoring carried out in the Bohemian Massif in underground areas with driven galleries, the trend displacements in the Josef gallery in Central Bohemia are around a hundredth of a mm/yr, and the Bedřich gallery in the Jizerské Mts. shows 0.02–0.05 mm/yr. Similar values in hundredths of a mm/yr have also been registered in the Grimsel underground facility in Switzerland. It must be mentioned, however, that the time over which the monitoring was carried out in the Bukov URF is incomparably shorter than that in the aforementioned sites, where it has been going on for 20–30 years. And if we consider the need to detect periods

where no displacement occurs on faults, or when it is decelerated or reversed, the values for the trends identified so far in the Bukov URF must be taken only as orientation values.

6.3 Results of numerical model

A “quasi-2D” model of the Bukov URF was prepared as part of the project as a 3D horizontal section located in the vicinity of the Bukov URF between approximately -563.5 m and -546.5 m. Plaxis 3D VIP software was used for the simulations.

The tectonic zones were incorporated in the model as weak rocks. The computation attempted a back-analysis of the measured movements by applying horizontal pressures on each block of intact rock.

The results yield information on the state of stress and pressure in the area, and the interpretation of disturbances by tectonic discontinuities. The model provided a general prediction of the measured strike-slips, where the predicted values were much in line with the measurements in qualitative terms, and correspond to the orders of magnitude in quantitative terms. It must also be mentioned that the measurements were influenced by a significant seasonal component (which was not simulated in the model), and the time span of the measurements was relatively limited to obtain information on long-term trends.

The model also gives another important output as it presents significant horizontal rock pressures in the area. To determine the measured displacements, a varying load of horizontal pressures between 5 MPa and 30 MPa had to be applied with the assumed geostatic value of 15 MPa. These values correspond well to the measurement of state of stress using various methods as presented in the geotechnical survey report for the area (Souček et al., 2018). The values of vertical stress, according to the survey, are close to the anticipated value of 15 MPa and have lower variance. The values of horizontal stress show a greater variance than those of vertical stress and range from 7 MPa to 38 MPa, which is highly consistent with the predicted values obtained from the numeric model, i.e., 5–45 MPa.

6.4 Recommendation for Following Procedures

In light of the results obtained so far in the Bukov URF, we recommend that regular monitoring with TM-71 spatial dilatometers installed in the premises of the Bukov 1 URF should continue. To be able to compare the values with the dynamics of displacements in the massif which is significantly less disturbed by discontinuities, approx. four TM-71 dilatometers should be installed in the new part of the facility, designated as Bukov 2. Prolongation of the monitoring will lead to a better understanding of the mechanism and dynamics of displacements registered at the specific structures equipped with dilatometers. It will also help to continuously improve the accuracy of the states of stress/strain, both at specific points in each structure and in greater scale in both parts of the Bukov URF. It will also help us to present improved correlations with other physical data obtained from the monitoring in the Bukov URF, and also with the results of the parallel monitoring of brittle structures carried out by the IRSM in the Grimsel (GTS) underground facility in Switzerland, where ten TM-71 devices are still in use now, or in similar underground premises in the Bohemian Massif, such as the Josef gallery or the gallery in Bedřichov. A longer dataset will also provide underlying data for the gradual improvement of the mathematical stress/strain model, the basis of which will be a model

prepared in stage 1 of the monitoring work carried out in 2018–2022 that was influenced by two major shortcomings: The time sequence of the displacement measurement was significantly affected by the seasonal component and isn't long enough to clearly identify long-term trends which the model should aim for, and the model was prepared in the so-called "quasi-2D" mode, which does not allow the interpretation of the vertical component of the movements. If the project continues, the preparation of a full 3D model is recommended.

References

AVRAMOVA-TACHEVA E., DOBREV N. (2007): ON THE APPLICATION OF 3D MONITORING METHODS OF ACTIVE FAULT AND GRAVITATIONAL MOVEMENTS. GEOLOGICA BALCANICA 36, 3-4, 13-20.

BÁRTA J., SLAVÍK L., VILHELM J., BELOV T., JIRKŮ J. (2020): PRŮBĚŽNÁ ZPRÁVA O POZNATCÍCH Z GEOFYZIKÁLNÍCH MĚŘENÍ NA PVP BUKOV – ETAPA 2. – MS SÚRAO, TZ 527/2020, PRAHA.

BRIESTENSKÝ M., ROWBERRY M. D., STEMBERK J., STEFANOV P., VOZÁR J., ŠEBELA S., PETRO Ľ., BELLA P., GAAL L., ORMUKOV CH. (2015): Evidence of a plate-wide tectonic pressure pulse provided by extensometric monitoring in the Balkan Mountains (Bulgaria). Geologica Carpathica 66, 5, 427-438.

BRIESTENSKÝ M., HOCHMUTH Z., LITTVA J., HÓK J., DOBROVIČ R., STEMBERK J., PETRO Ľ., BELLA P. (2018): Present-day stress orientation and tectonic pulses registered in the caves of the Slovensky kras Mts. (south-eastern Slovakia). Acta Geodynamica et Geomaterialia 15, 2, 93-103.

BUKOVSKÁ, Z., VERNER, K. a kol. (2017). Komplexní geologická charakterizace prostorů PVP Bukov, Technická zpráva 191/2017.

EVANS J.D. (1996): Straightforward Statistics for the Behavioral Sciences. Brooks/Cole Publishing, Pacific Grove, pp. 600.

GOSAR A., ŠEBELA S., KOŠŤÁK B., STEMBERK J. (2009): Surface versus underground measurements of active tectonic displacements detected with TM-71 extensometers in western Slovenia. Acta Carsol. 38, 213–226.

GOSAR A., ŠEBELA S., KOŠŤÁK B., STEMBERK J. (2011): On the state of the TM 71 extensometer monitoring in Slovenia: Seven years of micro-tectonic displacement measurements. Acta Geodyn. Geomat. 8, 4, 389–402.

HOPPE A., KOŠŤÁK B., KUHN G., LEHNÉ R., SIMONS U., STEMBERK J. (2015): Rezente Bewegungen an den Hauptrandverwerfungen im Nördlichen Oberrheingraben. Jber. Mitt. oberrhein. geol. Ver. 97, 321-332, Stuttgart.

HORÁK V. (2006): Puklinatost horninového prostředí. Brno, pp 16.

KLIMEŠ J., ROWBERRY M. D., BLAHŮT J., BRIESTENSKÝ M., HARTVICH F., KOŠŤÁK B., RYBÁŘ J., STEMBERK J., ŠTĚPANČÍKOVÁ P. (2012): The monitoring of slow-moving landslides and assessment of stabilisation measures using an optical-mechanical crack gauge. Landslides 9, 3, 407-415.

KONTNY B., CACOŃ S., KOŠŤÁK B., STEMBERK J. (2005): Methodic analysis of data obtained by monitoring micro-tectonic movements with TM-71 crack gauges in the Polish Sudeten. Acta Geodyn. Geomater. 2, 3, 57-67.

KOŠŤÁK B. (1969): A new device for in-situ movement detection and measurement. Experimental Mechanics 9, 374–379.

KOŠŤÁK B. (2006): Deformation effects in rock massifs and their long-term monitoring. Q. J. Eng. Geol. Hydroge., 39, 3, 249–258.

KOŠŤÁK B., MRLINA J., STEMBERK J., CHÁN B. (2011): Tectonic movements monitored in the Bohemian Massif. J. Geodyn. 52, 34-44.

KOŠŤÁK B., POPP K. (1966): Moiré strain gauges. Strain, 2, 5–16.

MARTÍ X., ROWBERRY M. D., BLAHŮT J. (2013): A MATLABs code for counting the moiré interference fringes recorded by the optical-mechanical crack gaugeTM-71. Computers & Geosciences 52, 164–167.

OSTER G., NISHIJIMA Y. (1963): Moiré patterns. Scientific American 208, 54–63.

STEMBERK J., BRIESTENSKÝ M., CACOŃ S. (2015): The recognition of transient compressional fault slow-slip along the northern shore of Hornsund Fjord, SW Spitsbergen, Svalbard. Polish Polar Research 36, 89-103.

STEMBERK J., BRIESTENSKÝ M., HARTVICH F., FUČÍK Z. (2020): Monitoring aktivity křehkých struktur PVP Bukov a dolu Rožná – průběžný monitoring a vyhodnocení 2. – MS SÚRAO, TZ 526/2020.

STEMBERK, J., BRIESTENSKÝ, M., HARTVICH F., FUČÍK Z. (2021). Monitoring aktivity křehkých struktur PVP Bukov a dolu Rožná – průběžný monitoring a vyhodnocení 3, Technická zpráva 571/2021.

STEMBERK, J., KOŠŤÁK, B., CACOŃ S. (2010): A tectonic pressure pulse and increased geodynamic activity recorded from the long-term monitoring of faults in Europe. Tectonophysics 487,1–12.

SOUČEK, K., VAVRO, M., STAŠ, L., KALÁB, Z., KONÍČEK, P. a kol. (2018). Komplexní geologická charakterizace prostorů PVP Bukov – část ii geotechnická charakterizace, závěrečná zpráva, Technická zpráva číslo 221/2018.

ŠEBELA S., TURK J., MULEC J., KOŠŤÁK B., STEMBERK J. (2009): Statistical evaluation of the 3D monitoring of displacements of Dinaric Fault zone in Postojna Cave, Slovenia. Acta Geodyn. Geomater. 6, 2, 163-176.

VYLAMOVÁ P., KOCMAN T., MUSIL R., PRŮCHA P. (2020): Hydrogeologický a hydrochemický monitoring podzemních a důlních vod v prostoru PVP Bukov, etapová zpráva za rok 2020. - MS SÚRAO, TZ 545/2021, Praha.

ZUNA M., HAVLOVÁ V., JANKOVSKÝ F., ŠVAGERA O., SOSNA K., GVOŽDÍK L., HOLEČEK J., ŘIHOŠEK J., HOFMANOVÁ E., KOČAN K., KRYL J., ZELINKOVÁ T., KOŘALKA S. (2021): VÝZKUM PUKLINOVÉ KONEKTIVITY V PVP BUKOV - PRŮBĚŽNÁ ZPRÁVA Č. 3. TZ 551/2021, SÚRAO, PRAHA.

SÚRAO | RADIOACTIVE WASTE REPOSITORY AUTHORITY

www.surao.cz